INCLUDING FREQUENCY-DEPENDENT IRON LOSSES IN ANALYTICAL MODELS OF INDUCTION MACHINES

Master's Thesis

Omar Laldin

Supervisor
Dr. Antero Arkkio

December 2008

Submitted in partial fulfillment for the degree of
Master of Science in Electrical Engineering

Department of Electrical Engineering
Faculty of Electronics, Communications and Automation
Helsinki University of Technology
Espoo, Finland

Abstract of the Master's Thesis

Helsinki University of Technology

Author:	Omar Laldin
Thesis Title:	Including Frequency Dependent Iron Losses in Analytical Models of Induction Machines
Date:	December 1, 2008 **Number of Pages:** 92

Department:	Electrical Engineering
Professorship:	S-17 Electrical Engineering (Electromechanics)
Supervisor:	Dr. Antero Arkkio

The objectives of the project are two-fold. First, appropriate models and tests should be developed to calculate core losses analytically and understand their dependency on frequency. Second, algorithms must be developed to solve the standard machine and core loss parameters.

To reach these objectives, small-signal models for the standard machine parameters will be utilised. Small-signal models including core loss parameters will be developed and verified. Core losses will be determined for a 37kW machine from Finite Element Analysis (FEA) at various voltage and frequency points. The results will be used to determine core loss parameters via the steady-state and developed small-signal models. Finally, a DC step voltage test will be utilised, along with an induction machine model at standstill, to determine machine parameters.

Three algorithms to determine the machine parameters, based on impulse voltage tests, are presented and compared. The first uses core loss resistance models with a fixed Steinmetz coefficient in small-signal and steady-state models of the induction machine. The second uses core loss resistance models with a variable Steinmetz coefficient. The third algorithm uses the same models used in the second algorithm; however, results of the step voltage tests are used to improve the speed of the algorithm. Furthermore, this algorithm allows all machine parameters to be determined independently. Specifically, the relationship between the stator and rotor leakage inductance need not be known.

The challenges faced in determining the aforementioned parameters will also be outlined. Ideas and algorithms to tackle these challenges will be presented. The use of the DC step voltage test to improve the parameter estimation process will be explained. A complete algorithm, using differential evolution and two forms of fixed-point iteration for determining the core loss parameters, will be outlined.

Keywords:	induction motor, circuit model, core losses, impulse response, step response, small-signal model, frequency dependency

Preface

This research work was carried out during the period between May 2008 and November 2008 at the Electromechanics Laboratory (which has recently merged into the Department of Electrical Engineering, Faculty of Electronics, Communications and Automation) in the Helsinki University of Technology.

First of all, I would like to thank my supervisor, Dr. Antero Arkkio, for giving me the chance to work with his lab and providing comments during the writing of the thesis. I would also like to express my most sincere gratitude to Dr. Emad Dlala, whose knowledgeable comments and guidance throughout the thesis made it a pleasure to learn from him. I also thank the remaining researchers at the laboratory, including Dr. Anouar Belachen for his useful comments, Jenni Pippuri for always willing clarify ideas with a smile, Dr. Anna-Kaisa Repo, whose earlier work inspired this thesis and finally, Katarzyna Fonteyn and Paavo Rasilo for the guidance they provided. I would also like to thank the staff members in the laboratory, including Ari Haavisto and Marika Schröder for helping in every way that they could. Finally, I have to thank Anita Bisi, the international student planning officer at our department, for all her help and wonderful conversations we have had since I moved to Finland.

From outside the university, there are numerous people to whom I am deeply grateful. I would like to thank Antti Keurulainen (along with the remaining employees of Bitville Oy) for providing support in innumerable ways during my time in Finland. I would also like to thank Laura Ojanen for giving me the opportunity to teach; doing so greatly strengthened my own understanding of various mathematical concepts. I am also grateful to the Academy of Finland and Ontario Student Assistance Program (in cooperation with the NSLSC) for their financial support.

I want to thank my family and friends for the support they have given over the years: my parents, Abdul Rahman and Aasia who have always been there, even from afar. I am still amazed at fate for directing me (rather fortunately) to my father's field. I look forward to seeing my sisters, Sidrah and Ayesha and my brother Ali once again. I also want to thank all the old friends from home, with whom it's been quite a ride. Specifically, I must thank Chris Jacobson for being a great friend for all these years and never letting me keep my head down for long.

On a final note, I want to express my deepest gratitude to Dr. Nick Stranges at GE Peterborough, who genuinely loves this field and really introduced me to electrical machines. Our countless hours of discussion made it a pure joy to work with and learn from him. His words of wisdom regarding machines theory still ring through my ears, nearly four years later:

> "Life is not that complicated…
> if its getting too complicated, then you're not doing something right."

Espoo, December 2008

Omar Laldin

Contents

List of Symbols

Symbols

Δ	perturbations in current or voltage
δ	skin depth
ψ	flux linkage
$\underline{\psi}_{\mathrm{m}}$	flux linkage across the air-gap
$\underline{\psi}_{\mathrm{r}}$	flux linkage experienced by the rotor
$\underline{\psi}_{\mathrm{s}}$	flux linkage experienced by the stator
μ	permeability of the material
ϕ	mutual flux across the air-gap
ρ	density of the material
σ	conductivity of the material
$\sigma(\ )$	standard deviation
θ	phase shift of the applied impulse
$\boldsymbol{\theta}'_{\mathrm{m}}$	approximate standard induction machine parameters
$\boldsymbol{\theta}'_{\mathrm{k}}$	approximate core loss parameters
ω_{r}	angular speed of the rotor in electrical radians
ω_{rm}	mechanical speed of the rotor
ω	electrical angular frequency under consideration
ω_{l}	fundamental electrical angular frequency
ω_{r0}	angular speed of the rotor at steady-state in electrical radians
a_{rel}	relative magnitude of the applied impulse
$\underline{a}$	$e^{\mathrm{j}\frac{2\pi}{3}}$ from the definition of a space-vector
B_{p}	peak flux density

CR user-defined crossover constant

d thickness of the lamination

f_{d} duration frequency of the applied impulse

f frequency under consideration

f_n frequency of the harmonic n

f_{1} fundamental frequency

f_{std} air-gap voltage function of the steady-state circuit, without core losses

f_{cl} air-gap voltage function of the steady-state circuit, with core losses

i_{s} stator current

I_{s} RMS value of stator current

I_{rand} random integer in [1,N]

$\underline{i}_{\mathrm{s}}$ space-vector of the stator current

$\underline{i}_{\mathrm{r}}$ space-vector of the rotor current

$\underline{i}_{\mathrm{m}}$ space-vector of the magnetising current

$\underline{i}_{\mathrm{Fe}}$ space-vector of the current through the core loss branch

I cost of a given test vector

k_{h} hysteresis loss coefficient

k_{e} eddy current loss coefficient

k_{p} pitch factor, defined as the sine of coil pitch divided by 2

k_{c} core loss coefficient

k_{e}^{*} eddy current loss coefficient for a non-sinusoidal supply

k_{ex}^{*} excess loss coefficient for the non-sinusoidal supply

K_{sk} effective thickness of the lamination

k coupling coefficient

$k_{\mathrm{ch}}^{'}$ approximate effective hysteresis loss coefficient

$k_{\mathrm{ce}}^{'}$ approximate effective eddy current loss coefficient

k_{ch} effective hysteresis loss coefficient

k_{ce} effective eddy current loss coefficient

L_{s} stator inductance

L_{m} magnetising inductance

$L_{\sigma \mathrm{s}}$ stator leakage inductance

L_{r} rotor inductance

$L_{\sigma \mathrm{r}}$ rotor leakage inductance

$L_{\gamma \mathrm{c}}$ core leakage inductance generated through circulating eddy currents

$L'_{\sigma \mathrm{s}}$ approximate stator leakage reactance

L'_{m} approximate magnetising reactance

N number of variables in a given population member (used in DE)

N_{c} number of turns per coil

n Steinmetz coefficient

n' approximate Steinmetz coefficient

P_{in} input power

P_{fw} friction and windage loss

P_{e} eddy current loss

P_{h} hysteresis loss

p number of pole pairs

P_{csh} hysteresis loss in the stator

P_{cs} core loss in the stator

P_{cse} eddy current loss in the stator

P_{cr} core loss in the rotor

P_{m} measured core loss

P_{c} calculated core loss

R_{s} stator resistance

R_{r} rotor resistance

$rand_{j,i}$ random real number in [0,1]

$R_{\mathrm{Fe}n}$ harmonic core loss resistance

$R_{\mathrm{Fe}}(\omega)$ core loss resistance at given angular velocity

R'_{r} approximate rotor resistance

s slip

s_l slip in terms of the synchronous speed of the electrical system

t_{st} starting time of the applied impulse

t_d duration of the applied impulse

t time

T_r rotor time constant

T_s stator time constant

$\mathbf{u}_{j,i,g}$ *i*th variable in the *j*th trial vector of the *g*th generation

$\underline{u}_s$ space-vector of the supply voltage

$\underline{u}_r$ space-vector of the rotor voltage

$\hat{u}_\varphi$ peak phase voltage

U_{llrms} line to line RMS voltage

u_{sx} voltage in stator phase *x*

$\mathbf{v}_{j,i,g}$ *i*th variable in the *j*th mutant vector of the *g*th generation

V_m air-gap voltage

V_s stator voltage magnitude for a DC step voltage test

V_{m_0} initial guess for air-gap voltage

$\mathbf{x}_{j,i,g}$ *i*th variable in the *j*th parent vector of the *g*th generation

X_{Zi} error of the *i*th test vector, determined from admittance curve

$\overline{X}_Z$ mean of errors from test vectors, determined from admittance curve

X_{Pi} error of the *i*th test vector, determined from core losses

$\overline{X}_P$ mean of errors from test vectors, determined from core losses

Y_m measured admittance values in frequency range of interested

Y_c calculated admittance values in frequency range of interested

Subscripts

0 steady-state values

i *i*th test value

$_0$ initial guess

1 fundamental values

Acronyms

DE	Differential Evolution
FE	Finite Element
FEA	Finite Element Analysis
PWM	Pulse Width Modulated
SLL	Stray Load Loss

List of Figures

List of Tables

Chapter 1
Introduction

The thesis is a subset of a larger project being conducted by the Electromechanics Group between January 2008 and December 2010. The project is being carried out in cooperation with the Power Electronics Group in TKK, with some collaborative efforts from Technische Universtät Darmstadt and ETH Zurich. The aim of the project is to develop a control algorithm that minimises the total loss in both the variable speed induction machine (induction machine) and its frequency converter. For this task, the controller requires adequate models of losses in the machine.

1.1 Aim of the Thesis

The aim of the thesis is to include the frequency-dependent iron losses in the analytical models of induction machines. Appropriate models and tests must be determined to allow the iron losses to be determined analytically. In addition, algorithms need to be developed to solve the machine and core loss parameters based on the outlined tests.

The thesis builds the groundwork for determining core and stray load losses for Pulse Width Modulated (PWM) supplies operating at various switching frequencies. Recommendations for future work are given in Chapter 6.

1.2 Scope and Definitions

Prior to pursuing any investigations regarding iron losses, it is important to define, precisely, the meaning of the term. IEEE Standard 112 defines core losses as the result

obtained by "…subtracting the value of the friction and windage loss … from the input power minus stator I^2R loss", during a no-load test.

$$P_c = P_{in} - P_{fw} - I_s^2 R_s \quad (1)$$

The core losses in the machine are a result of hysteresis and circulating eddy currents in the machine laminations. As such, they are usually modelled as a sum of the two [(Sousa et al., 1992) & (Honsinger, 1980)]:

$$P_c = P_h + P_e \quad (2)$$

It should be noted that Bertotti (1988) added a third component to the above. He termed this the excess loss component, resulting from the "competition between the external magnetic field, applied uniformly in the sample, and highly inhomogeneous local centerfields due to eddy currents and microstructural interactions." Depending on the material and the operating conditions under consideration, this component can be almost as high as the eddy current component (Bertotti, 1988).

The stray-load losses, however, contain numerous components and as such, are described in a variety of ways in the literature. The IEEE Standard 112 defines them as "that portion of the total loss in a machine not accounted for by the sum of the friction and windage loss, the stator I^2R loss, the rotor I^2R loss and the core loss." The standard generally agrees with the definition used by others [(Olin, 1912); (Alger et al., 1957); (Bird, 1964) & (Jimoh et al., 1985a)]. It is apparent that this definition includes losses otherwise unaccounted for once the machine is loaded; they include both iron and copper losses. In effect, the core losses and part of the stray-load losses total the iron losses in the loaded machine.

Schwarz (1964) provided a comprehensive list of stray-load loss components, their origin, as well as their type and location. The list is reprinted below.

Table 1: Stray-Load Loss Components (Schwarz, 1964)

Components	Origin	Type and Location
Surface losses	Gap leakage (harmonic) flux	Stator and rotor core losses
Tooth-pulsation losses	Gap leakage (harmonic) flux	Stator and rotor core losses
Tooth-pulsation, squirrel-cage, circulating current losses	Gap leakage (harmonic) flux	Rotor I^2R loss
Stator-harmonic, squirrel-cage, circulating current losses	Gap leakage (harmonic) flux	Stator I^2R loss
Stator-slot eddy current losses	Slot leakage flux	Stator I^2R loss
Rotor-slot eddy-current losses	Slot leakage flux	Abnormal rotor I^2R loss at high slip only
Stator-overhang eddy-current losses	Overhang leakage flux	Stator core loss
Rotor-overhang eddy-current losses	Overhang leakage flux	Abnormal rotor core loss at high slip only

It is obvious that four of the above components occur in the copper and four occur in the iron. The aim of the thesis was to determine the losses in the iron and as such, the methodology did not allow the copper components of the stray-load losses to be determined. Furthermore, an attempt was made to determine the iron components of the stray-load losses by running FE tests with blocked rotor conditions. Under these conditions, however, the pulsation losses listed above are not included. Running FE tests at rated "slip" for various supply frequencies was foreseen to produce meaningless results. As such, the remaining work is focused on the core losses described earlier. Note that the thesis uses definitions for core losses as outlined in IEEE Standard 112.

1.3 Outline of the Thesis

The thesis is outlined as follows:

Chapter 1 provides the introduction to the thesis. The goals and background of the larger project are outlined. The aim of the thesis as a subset of the project is discussed. The scope of the work and appropriate definitions are provided.

Chapter 2 discusses the overall methodology of the thesis. The chapter is meant to provide the context for the more detailed methods outlined throughout the thesis.

Chapter 3 presents a literature review of various tools and concepts used during the thesis. The standard steady-state, dynamic and small-signal models of induction machines are presented. Steady-state and dynamic models of induction machines with core losses are also considered. The procedures for determining the standard machine parameters using both an impulse and a DC step response test are outlined. Analytical models for core losses and methods to determine them using FEA are presented.

Chapter 4 provides the author's contributions to the work. A small-signal model including the core loss parameters is developed. Core loss resistance model for a variable Steinmetz coefficient is derived. Algorithms to determine the parameters for the various models are outlined. A combined method to determine the machine leakage inductances independently is presented.

Chapter 5 provides the results of the thesis. The core losses and their associated resistance values are presented and compared. Similarly, the admittances using the small-signal models are calculated and presented. The results of the DC step voltage test are also presented. The parameters used for all algorithms, their calculation times and their outputs are provided.

Chapter 6 concludes the thesis by discussing the accuracy of the models and the convergence characteristics of the algorithms. A summary of the thesis is provided. The final proposed algorithm is outlined. A self-evaluation by the author and recommendations for future work are also presented.

Chapter 2

Methodology

As stated earlier, the aim of the thesis is two fold: to incorporate iron losses into the induction machine models and to establish a working mechanism to estimate the parameters for a given machine. The approach for the study is outlined below in reference to Figure 1.

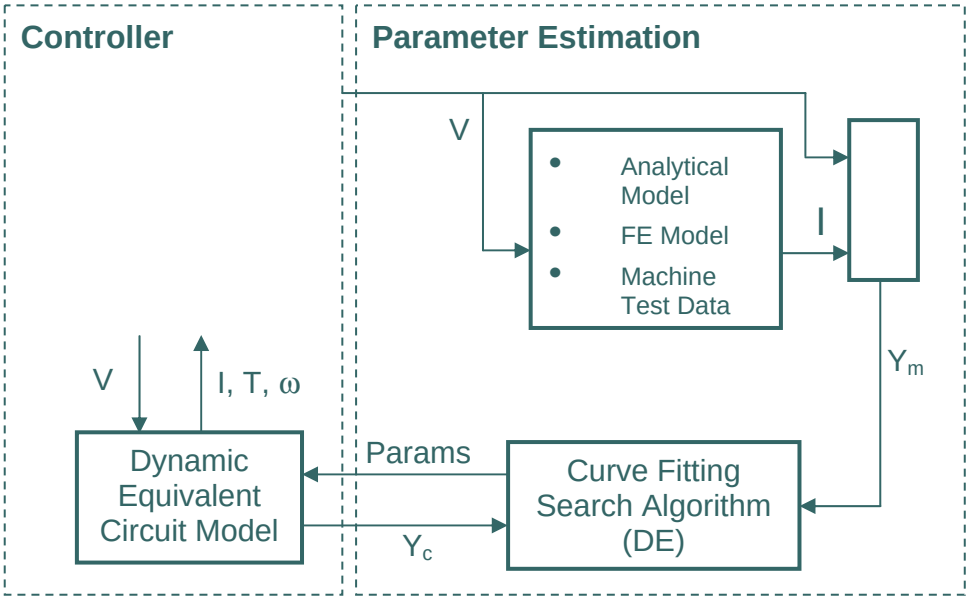

Figure 1: Parameter Estimation Process Overview

The dynamic model is to be implemented in a controller for a PWM frequency converter. Once connected to an induction machine, the controller should be able to determine the parameters for the machine by applying a specified voltage and reading the corresponding current drawn by the machine. In this document, the impulse response test and the step voltage tests are used.

In the case of the impulse response test, the applied voltage and corresponding current are transformed to their frequency domain representations and admittances are obtained for the frequency range under consideration. This measured admittance (Y_m) is then stored for use by the curve fitting algorithm. The Differential Evolution (DE) algorithm was used for this study as it exhibits efficient global convergence characteristics for higher order multivariate searches, with solution spaces containing local minima. The algorithm estimates parameters used by the dynamic circuit model to obtain a calculated admittance (Y_c) over the frequency range. The calculated admittance is compared with the measured admittance and the algorithms iterates until Y_c fits Y_m, at which point the parameters are stored in the controller.

It is to be noted that initially, the voltage impulse was applied to an analytical small-signal equivalent circuit model of a 37kW caged induction machine. The model was developed using space-vector theory. Doing so allowed the remaining system to be implemented and operating parameters (e.g. for the search algorithm) to be established. The aim is to eventually replace the analytical model with actual test data from the machine. However, as will be explained, doing so will require the development of further tests or the measurement of outputs other than the stator current.

During the thesis, Finite Element Analysis (FEA), modelling hysteretic materials, was used to determine results for the impulse response tests. The FE models were also used to determine the steady-state core losses for a variety of voltage and frequency points. The purpose of running these tests was to get a better understanding of the effect of frequency on the core losses. The tests were required as the effects of core losses on stator current turned out to be small.

As a comparison, the standard parameters were also calculated using a DC step voltage test. A combination of the step voltage test and the impulse response test is then used to determine all required parameters for the caged induction machine.

Chapter 3

Literature Review

3.1 Overview

A large variety of material was studied and utilised for the thesis. In a two part publication, Jimoh et al. (1985a, 1985b) tackled the problem of defining, calculating and reducing stray load losses (SLLs) in induction machines. Alger et al. (1957) described physical origins of SLLs and presented approximate calculation models. Numerous publications have discussed measurement techniques of SLLs and discussed their effects on machine performance [(Olin, 1912); (Koch, 1932); (Morgan et al., 1939); (Chalmers et al., 1958); (Bird,1964) & (Spooner, 1982)]. Honsinger (1980) gave a very thorough analysis of inverter-driven induction machines, where he studied both the machine and the inverter, eloquently explaining frequency-dependent behaviour in both. In a collaborative effort funded by the US Environmental Protection Agency, Souse et al. (1992) developed circuit models for the converter as well as the induction machine, which were used to calculate iron losses. Levi (1994) studied iron losses resulting from indirect rotor flux oriented control and later (Levi et al., 1995) studied circuit models which include SLLs in induction machines. Mthombeni & Pillay (2003) developed core loss models for induction machines operating with PWM supplies and Manyage et al. (2007) proposed an improved model for the same.

Repo (2006) developed a method to estimate machine parameters from impulse response tests. She used parameterised small-signal models, thereafter with saturation and skin effects included (2008), to predict the impulse response of the induction machine. A voltage impulse had been applied to a time stepping FE model and the results used to estimate the parameters. The work prompted the use of such methods to determine iron loss parameters and is expected to aid in determining their dependence on converter

frequencies. However, the model used by Repo did not include iron losses in the field analysis. Dlala (2008b) developed a magnetodynamic vector hysteresis model to be used in determining iron losses in the machine. The model is applicable to a wide range of frequencies and was thus indispensible in studying iron loss behaviour over various frequency points. Recently, Dlala and Repo's works were combined to allow an impulse response to be studied, in light of iron losses.

Belloc et al. (2006) provided a time-domain step voltage response method to identify machine parameters at standstill. The simplicity of the method allows fast computation, making it an attractive option for use in this thesis. Moon et al. (1993) used a time-discretised state space model, with the Maximum Likelihood estimation algorithm, to determine current response to a step voltage. Yamamoto et al. (2004) investigated five different methods to determine machine parameters: DC decay, two types of step response and two types of pulse response methods. Sellschopp et al. (2007) and Couto & Aguiar (1998) provided frequency domain models for similar purposes.

3.2 Differential Evolution

During the thesis, the differential evolution search algorithm (Storn & Price, 1997) was used extensively for a variety of reasons. As such, the basics of the algorithm are presented here. The algorithm belongs to the family of evolutionary algorithms and is based on patterns observed in biological systems.

The algorithm is initialised by creating a set of n solution vectors, forming the total "population". The upper and lower limits for each variable in the solution vector are predefined by the user.

The sequence of the algorithm is given in the following figure.

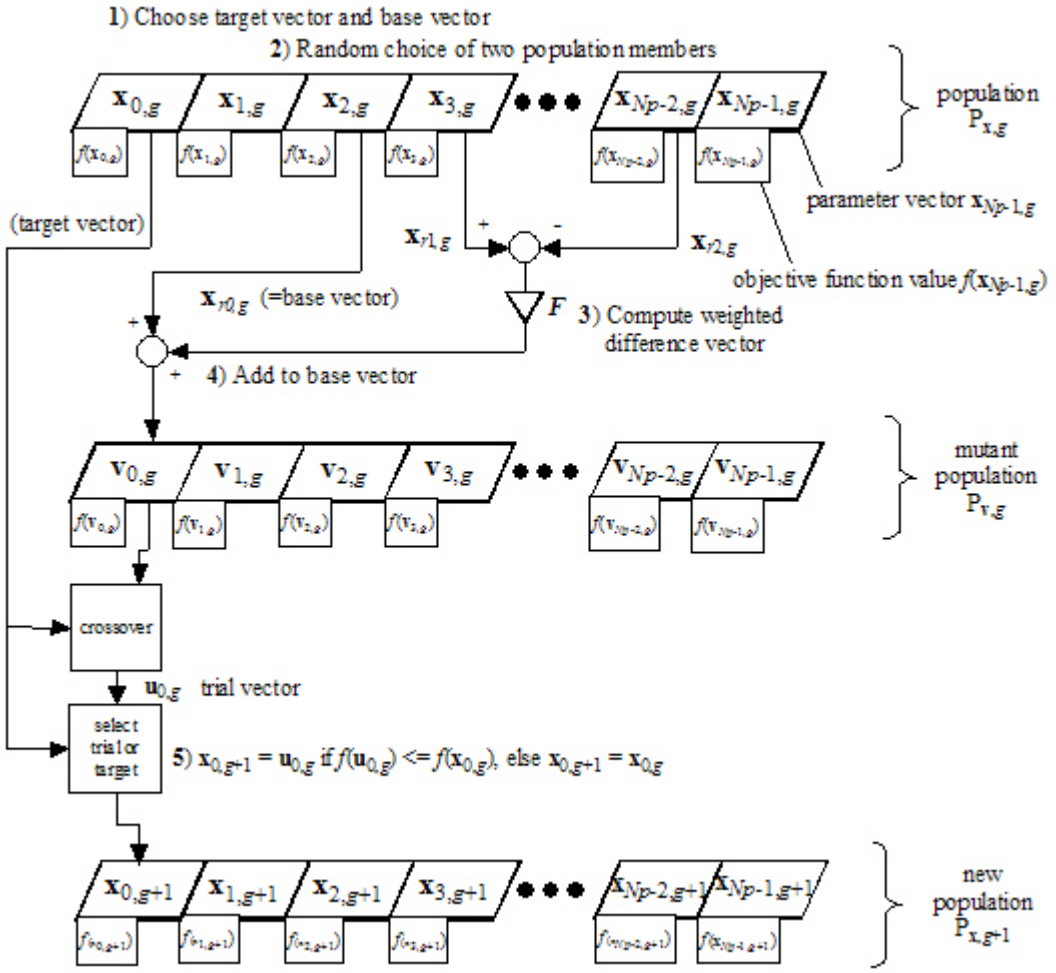

Figure 2: Differential Evolution Overview (Storn, 2008)

The parent population goes through a series of mutation, recombination and selection steps to produce the offspring set. First, "target" and "base" vectors are selected. The target vector is the vector to be overwritten. The base vector is the vector to be mutated. A weighted difference between two additional random members is used to form the mutation, which is then added to the base vector. When repeated for each member of the parent population, this sequence creates the "mutant" population, which is then exposed to some crossover with the target (parent) vector to obtain a trial vector. The cross over is defined below.

$$\mathbf{u}_{j,i,g} = \begin{cases} \mathbf{v}_{j,i,g} & \text{if } rand_{j,i} \le CR \text{ or } i = I_{\text{rand}} \\ \mathbf{x}_{j,i,g} & \text{if } rand_{j,i} > CR \text{ and } i \ne I_{\text{rand}} \end{cases} \tag{3}$$

where

j is the population member index
i is the index for a variable within a member
g is the generation index
$rand_{j,i}$ is a random real number in $[0,1]$
CR is the user-defined crossover constant
I_{rand} is a random integer in $[1, N]$
N is the number of variables in a given member
$\mathbf{u}_{j,i,g}$ is the trial vector
$\mathbf{v}_{j,i,g}$ is the mutant vector
$\mathbf{x}_{j,i,g}$ is the parent vector

Note that implementing I_{rand} ensures that the trial vector is not identical to the parent vector. The cost function of the trial vector is then compared with the cost function of the parent vector; the one with the higher cost is discarded and the other is chosen as the offspring vector. Once completed for all population members, the iteration continues for following generations until a given error limit is reached. A more thorough analysis of the DE algorithm is available online (Storn & Price, 2007).

3.3 Standard Circuit Models

Prior to the addition of iron losses, it is pertinent to describe the standard steady-state and dynamic circuit models used to represent the induction machine. In addition, the associated small-signal model and the characteristics of the applied voltage impulse, as developed by Repo (2006), are described here. As will be described in Chapter 4, these simplified models are used to calculate voltage, current and flux approximations that are later refined by the models incorporating iron losses.

The steady-state and dynamic circuit models for the induction machine are shown in the following figures.

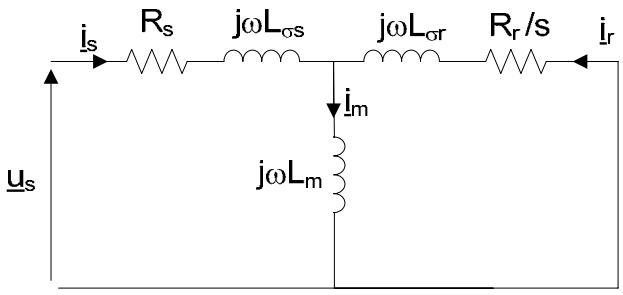

Figure 3: Steady-State Circuit Model of an Induction Machine

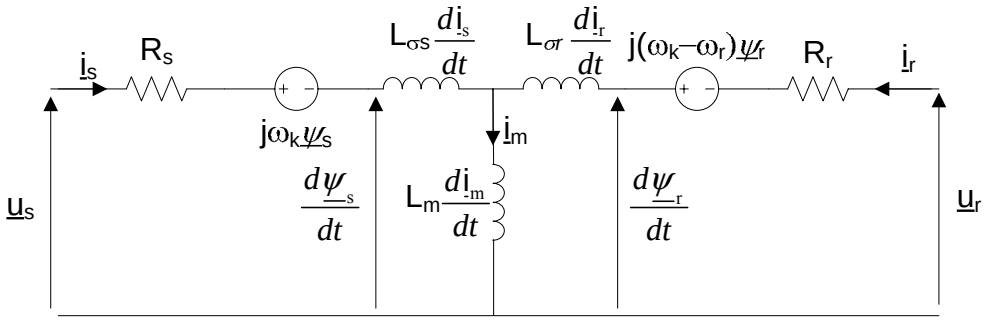

Figure 4: Dynamic Circuit Model of an Induction Machine

The above circuit model produces the following space-vector equations in the stator reference frame.

$$\underline{u}_s = R_s \underline{i}_s + \frac{d\underline{\psi}_s}{dt} \tag{4}$$

$$0 = R_r \underline{i}_r + \frac{d\underline{\psi}_r}{dt} - j\omega_r \underline{\psi}_r \tag{5}$$

$$\underline{\psi}_s = L_s \underline{i}_s + L_m \underline{i}_r \tag{6}$$

$$\underline{\psi}_r = L_m \underline{i}_s + L_r \underline{i}_r \tag{7}$$

$$\underline{i}_m = \underline{i}_s + \underline{i}_r \tag{8}$$

where,

$$L_s = L_{\sigma s} + L_m \tag{9}$$

$$L_r = L_{\sigma r} + L_m \tag{10}$$

$\underline{u}_\mathrm{r}$ has been set to 0 for a caged rotor
$\omega_\mathrm{r}\,(=p\omega_\mathrm{rm})$ is the speed of the rotor, in electrical radians
ω_rm is the mechanical speed of the rotor
p is the number of pole pairs

If the stator resistance is known (e.g. with a DC voltage test), (4) to (10) represent a model with four parameters to be estimated.

3.4 Impulse Response Test

A voltage impulse is applied during steady-state operating conditions, resulting in transient behaviour near the steady-state operation point. As such, the impulse can be considered a small-signal above the steady-state voltage and is defined as follows (Repo, 2006).

$$\underline{u}_\mathrm{s}+\Delta\underline{u}_\mathrm{s}=\left|\underline{u}_\mathrm{s}\right|e^{\mathrm{j}\omega t}+\left|\Delta\underline{u}_s\right|e^{\mathrm{j}(\omega t+\theta)} \tag{11}$$

where

$$\left|\Delta\underline{u}_\mathrm{s}\right|=\begin{cases} a_\mathrm{rel}\left|\underline{u}_\mathrm{s}\right|\sin^2\left(2\pi f_d t\right) & t_\mathrm{st}\le t\le t_\mathrm{st}+t_\mathrm{d} \\ 0 & \text{otherwise}\end{cases}$$

t_st is the start time of the impulse (12)
t_d is the duration of the impulse

The above definition for the magnitude of the impulse excites frequencies between -400Hz and 400Hz, when f_d is 200Hz and t_d is 5ms. The steady-state voltages are then subtracted from the applied voltage to obtain the voltage impulse alone.

The impulse results in minor perturbations in the currents and the flux. However, the measured current will also include the steady-state current component containing harmonic content due to machine geometry. To obtain the current transient due to the impulse alone, the steady-state current is subtracted from the output current of the induction machine. Repo (2008) also noticed that the effect of saturation is cancelled out when, instead of subtracting steady-state quantities, the test results of an applied impulse with a phase shift of 90° are used.

The Fourier transform of both the voltage impulse and current response are obtained. The frequency domain current is then divided by the frequency domain voltage to obtain the frequency domain admittance. The parameters of the small-signal model are determined by fitting the calculated and measured admittance curves via the DE algorithm. The standard small-signal model for the induction machine is given below.

3.5 Standard Small-Signal Model

Small-signal models are used to study the behaviour of the voltage and current changes. Dynamic models are used to develop the small-signal model for the machine (Repo, 2006). In the Laplace domain, the small-signal model, after subtracting the effects of the steady-state voltage and current parameters, results in the following system of equations (Repo, 2006).

$$\Delta \underline{u}_s = R_s \Delta \underline{i}_s + j\omega\left(L_s \Delta \underline{i}_s + L_m \Delta \underline{i}_r\right) \tag{13}$$

$$0 = R_r \Delta \underline{i}_r + j\omega\left(L_m \Delta \underline{i}_s + L_r \Delta \underline{i}_r\right) - j\omega_{r0}\left(L_m \Delta \underline{i}_s + L_r \Delta \underline{i}_r\right) \tag{14}$$

where

it is assumed that the change in rotor speed due to the impulse is negligible
$j\omega$ forms the Laplace transform variable
ω_{r0} is the steady-state angular velocity of the rotor, in electrical radians

Equations (13) and (14) must be rearranged to get the current-to-voltage (or admittance) ratio. Rearranging (13) for $\Delta \underline{i}_r$ and inserting into (14) gives

$$\Delta \underline{i}_r = \frac{j(\omega_{r0} - \omega) L_m \Delta \underline{i}_s}{R_r + j(\omega - \omega_{r0}) L_r} \tag{15}$$

$$\Delta \underline{u}_s = R_s \Delta \underline{i}_s + j\omega\left(L_s \Delta \underline{i}_s + L_m \frac{j(\omega_{r0} - \omega) L_m \Delta \underline{i}_s}{R_r + j(\omega - \omega_{r0}) L_r}\right) \tag{16}$$

Finally, rearranging (16) for the admittance yields (Repo, 2006)

$$\frac{\Delta \underline{i}_s}{\Delta \underline{u}_s} = \left[\frac{R_r + j\omega L_r - j\omega_{r0} L_r}{\omega^2\left(L_m{}^2 - L_s L_r\right) + \omega\left(jL_s R_r + jR_s L_r + \omega_{r0} L_s L_r - \omega_{r0} L_m{}^2\right) + R_s R_r - j\omega_{r0} R_s L_r}\right] \tag{17}$$

3.6 Core Power Loss Models

To compute the core power loss, various models have been presented in the literature. As a starting point, the model used by Sousa et al. (1992) is considered first. It is assumed here that core losses due to mutual flux harmonics are governed by the same principle that causes the losses by the fundamental mutual flux (i.e. similar equations can be used for both).

To calculate the losses due to the fundamental frequency in the stator core, it is assumed that the hysteresis loss is proportional to the frequency and eddy current loss is proportional to the frequency squared. Both are assumed to be proportional to the mutual flux squared.

$$P_{cs} = P_{csh} + P_{cse} = k_h f \phi^2 + k_e f^2 \phi^2 \tag{18}$$

where

P_{csh} is the hystereris loss in the stator
P_{cse} is the eddy current loss in the stator
k_h is the hysteresis coefficient
k_e is the eddy current coefficient
ϕ is the mutual flux in the air gap

It should be noted that the hysteresis loss had empirically been determined to be proportional to the mutual flux raised to the power of 1.7 (Jones, 1967). Steinmetz (1892) had determined the value of this constant (appropriately named the Steinmetz coefficient) to be 1.6 (reprinted in Manyage et al., 2007). However, it was found to be inapplicable to all flux density ranges for all materials (Chen & Pillay, 2002). Furthermore, Hinkkanen (2008), suggests this constant should not be preset. The question of the mutual flux exponent to be used for hysteresis loss will be addressed shortly.

The core loss in the rotor is modeled in a similar manner. However, the rotor current exhibits a frequency of slip times the supply frequency. The core loss in the rotor is given as

$$P_{cr} = k_h s f \phi^2 + k_e (sf)^2 \phi^2 \tag{19}$$

The total core loss is therefore

$$P_c = P_{cs} + P_{cr} = k_h f\phi^2 + k_h s f\phi^2 + k_e f^2\phi^2 + k_e s^2 f^2\phi^2$$
$$= \left[k_h \frac{(1+s)}{f} + k_e \left(1+s^2\right) \right] f^2\phi^2 \tag{20}$$

Air-gap flux ϕ is related to air-gap voltage V_m by

$$V_m(t) = V_m \sin\omega t = \frac{d\psi(t)}{dt} = \omega\psi \sin\omega t \tag{21}$$

$$\psi = \frac{V_m}{\omega} = N_c k_p \phi \tag{22}$$

$$\phi = \frac{V_m}{N_c k_p \omega} = \sqrt{k_c}\frac{V_m}{\omega} \tag{23}$$

Inserting the mutual flux relationship into the equation for core loss:

$$P_c = \frac{k_c}{4\pi^2}\left[2\pi k_h \frac{(1+s)}{\omega} + k_e \left(1+s^2\right) \right] {V_m}^2 \tag{24}$$

Therefore, the equivalent core loss resistance R_c can be derived as

$$R_{Fe} = \frac{1}{\frac{k_c}{4\pi^2}\left[2\pi k_h \frac{(1+s)}{\omega} + k_e \left(1+s^2\right) \right]}$$
$$= \left[k_{ch} \frac{(1+s)}{\omega} + k_{ce} \left(1+s^2\right) \right]^{-1} \tag{25}$$

where

$$k_{ch} = \frac{k_c k_h}{2\pi}, k_{ce} = \frac{k_c k_e}{4\pi^2}$$

It is assumed here that the coefficients k_e and k_h are not frequency dependent. However, the behaviour of these coefficients needs to be studied more thoroughly (Manyage et al., 2007).

At this point, it may be relevant to review the meaning of the frequency ω. For a 3-phase, Y-connected RL series circuit, with a 3-phase AC voltage source, the following relationship is obtained using space-vectors:

$$\underline{u}(t) = R\underline{i}(t) + L\frac{d\underline{i}(t)}{dt} \tag{26}$$

Assuming zero initial conditions, the Laplace transform is obtained as follows:

$$\underline{U}(s) = R\underline{I}(s) + sL\underline{I}(s) = (R + sL)\underline{I}(s) = Z(s)\underline{I}(s) \tag{27}$$

If the Fourier transform is considered, where $s = j\omega$, the following representation results.

$$\frac{\underline{U}(\mathrm{j}\omega)}{\underline{I}(\mathrm{j}\omega)} = Z(\mathrm{j}\omega) = R + \mathrm{j}\omega L = R + \mathrm{j}X(\omega) \tag{28}$$

Note that although the Fourier transforms of the voltages and currents themselves contain natural poles at the supply frequency, the impedance has a definite complex value. Let the impedance in (28) represent a power line, with a frequency-dependent resistance exhibiting the skin effect phenomenon (Cochran, 1989). A simple model (Jeon, 2007) for this skin effect adjusts the resistance in the following manner.

$$R(\omega) = R\sqrt{\frac{\omega}{\omega_1}} \tag{29}$$

The impedance is then represented by

$$Z(\mathrm{j}\omega) = R\sqrt{\frac{\omega}{\omega_1}} + \mathrm{j}\omega L = R(\omega) + \mathrm{j}X(\omega) \tag{30}$$

In (30), the resistance value changes in response to the applied frequency. The behaviour is similar to the behaviour of the core loss resistance defined in (25). Note that using this resistance in the time-domain model either requires a transformation to the time-domain (Nakamura, 2006), or prior knowledge of the frequency. Although the currents exhibit nearly sinusoidal behaviour at the fundamental for PWM excitation, numerous harmonics are present. These harmonics will experience a core loss resistance based on the definition given in (25). It is therefore far-sighted to carry forward with this definition, even if the supply frequency will be constant throughout this thesis.

For harmonic frequencies significantly greater than the fundamental, the slip in terms of the harmonic frequency may be considered to be 1 (i.e. $s \approx 1$). The equivalent core loss resistance $R_{\mathrm{Fe}n}$ at a harmonic frequency f_n is then

$$R_{\mathrm{Fe}n} = \frac{1}{2k_{\mathrm{c}}\left[\frac{k_{\mathrm{h}}}{f_n} + k_{\mathrm{e}}\right]} = \frac{0.5}{k_{\mathrm{c}}\left[\frac{k_{\mathrm{h}}}{f_n} + k_{\mathrm{e}}\right]} \tag{31}$$

Note that, as stated earlier, Sousa et al. (1992) make the assumption that fundamental and harmonic fluxes result in core losses that may be modelled similarly. However, it should be noted that these fluxes flow in very different paths in the machine.

When the frequency being considered is near the fundamental supply frequency,

$$s = \frac{f - (1 - s_1) f_1}{f} \tag{32}$$

where

f is the supply frequency under consideration
f_1 is the fundamental supply frequency
s_1 is the slip in terms of the fundamental

Honsinger's (1980) analysis of core losses is virtually identical to the one just outlined. However, he does state that ϕ is the mutual flux corrected for the eddy current reaction flux. Although the correction is trivial at 60 Hz, the phenomena is part of the excess loss component discussed earlier and requires further investigation for higher frequencies.

As mentioned earlier, Manyage et al. do not give a specific value for the Steinmetz coefficient (chosen to be 2 above). However, they point out that the "accepted value" of 1.6 does not hold under certain conditions. As such, an improvement in the model is inherent if the Steinmetz coefficient is left as an unknown machine-specific parameter. The core loss (in this case, per unit mass) then becomes

$$P_c = k_h f B_p^{\,n} + k_e f^2 B_p^{\,2} \tag{33}$$

where

P is the average loss per unit mass at frequency f
B_p is the peak flux density
n is the Steinmetz constant

The cited work provides additional improvements to the above core loss models; the proposed core loss model is given below.

$$P_c = P_h\left(f, B_p\right) + k_e^*\left(f\right)\left(\frac{dB}{dt}\right)^2 + k_{ex}^*\left(f, B_p\right)\left|\frac{dB}{dt}\right|^{1.5} \tag{34}$$

For sinusoidal supplies, (34) reverts to

$$P_c = P_h\left(f, B_p\right) + k_e\left(f\right) f^2 B_p{}^2 + k_{ex}\left(f, B_p\right) f^{1.5} B_p{}^{1.5} \tag{35}$$

Note that k^*_{ex} and k^*_{e} above are also defined so as to revert to k_{ex} and k_e for sinusoidal supplies.

Manyage et al. include the excess loss component, dependent on the peak flux density raised to 1.5, as proposed by Bertotti (1988). To allow for non-sinusoidal supplies, the eddy current and excess loss components are also modified to become dependent on *dB/dt*. The hysteresis loss function above is defined such that its ratio over frequency is a fourth order polynomial, the parameters of which are then determined by curve fitting techniques. The coefficient of the eddy current loss is modelled by utilising the skin depth equation, calculated at the appropriate frequency.

$$\delta = \sqrt{\frac{1}{f\pi\mu\sigma}} \tag{36}$$

If the skin depth given by (36) is greater than the thickness of the steel lamination, the classical equation for k_e is used, where $k_e = \frac{\sigma\pi^2 d^2}{6\rho}$. Otherwise, $k_e = \sigma\pi^2 K_{sk}$, where K_{sk} is the effective thickness and is defined as

$$K_{sk} = \left(\frac{\delta\left(e^{-\frac{2\delta - d}{\delta}} - e^2\right)}{e^{\frac{d}{\delta}} + 1} \right)^2 \tag{37}$$

Note that the eddy current loss coefficient requires knowledge of the material and laminations.

The excess loss is fitted to a curve, which was obtained from measured results (by subtracting the hysteresis and eddy current loss from the total core loss). It was discovered that the excess loss follows a natural logarithmic curve, the parameters for which were also determined by curve-fitting (Manyage et al., 2007).

To summarise, there are three sets of modifications to core loss models described: leaving the Steinmetz coefficient as an unknown variable, adding the excess loss and refining the frequency dependency of the eddy current and excess loss coefficients. Finally, for the case of non-sinusoidal supplies, derivatives of the flux density can be used.

During the course of this thesis, the complexity of the model was raised as required. Therefore, the simplest model providing adequate results was implemented.

3.7 Modelling Core Losses using FEA

As previously stated, core losses were determined using FE models (developed by Dlala, 2008) for various supply voltages and frequencies. The mesh used for the models consisted of 2nd order elements and was set to be changeable for the rotating rotor. The complete parameters used for the FE runs are given in Appendix B. The characteristics of the 37kW caged induction machine are given in Appendix C. The mesh used is shown in the figure below.

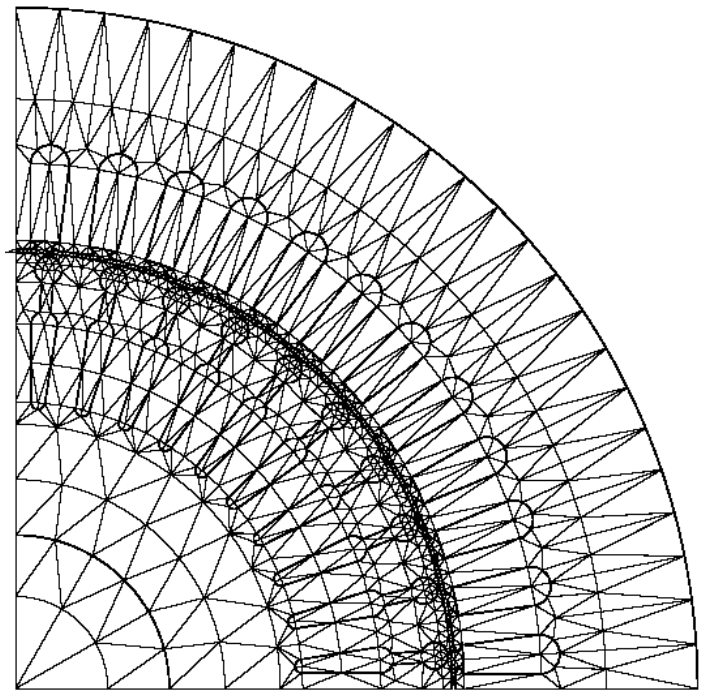

Figure 5: Finite Element Mesh for the 37kW Caged Induction Machine

The core losses are then determined for the voltage and frequency points (given in Appendix A) using hysteretic material models (Dlala, 2008a). Dlala (2008b) presents a simplified iron loss model for laminated cores, where the magnetization curves and loop shapes are first evaluated. The hysteresis, excess and classical eddy-current losses are then determined by calculating the loop areas. The model implements the Preisach model to determine rotational losses. The Fixed-Point Method is used to handle the emergent nonlinear behaviour of the model; it replaces the previously used Newton-Raphson

Method. Time-stepping vector analysis is then conducted using the Crank-Nicholson Method. Note that sinusoidal voltages were applied to the machine, with a time step of 1.0E-5 seconds and a simulation time of 5.0E-2 seconds. A plot of the flux and the core loss density is given in the following figure.

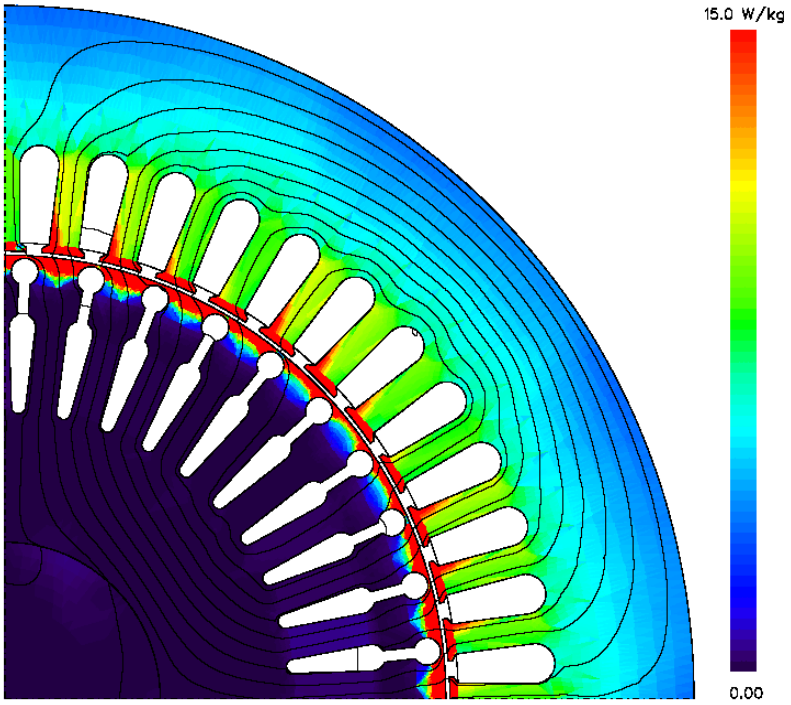

Figure 6: Flux and Core Loss Density Plot for the 37kW Caged Induction Machine

It is clear from the above figure that the majority of the losses occur in the stator teeth and tooth tips. There is also significant loss in the rotor tooth tips. The rotor experiences mostly uniform flux and as such the losses in the rotor body are negligible. The rotor teeth experience significant flux pulsations and as such, represent the loss due to the flux (and therefore, current) harmonics. Although the stator tooth-tips experience similar zig-zag fluxes, the remaining core experiences a significant amount of the fundamental flux. As the majority of the stator mass is in the remaining core, the core losses in the stator are largely affected by the fundamental component of the stator current.

3.8 Circuit Models with Core Losses

The inclusion of core losses in the equivalent circuit will be discussed here. As stated earlier, Levi (1994) investigated the applicability of a model suggested by Boldea (1987) to indirect rotor flux oriented induction machines. The model accounted for the core losses by adding an RL series circuit in parallel with the magnetising branch of the induction machine. Similar models are reported in [(Hildebrand & Roehrdanz, 2001);

(Honsinger, 1980); (Loddick, 1996);(Barnes and Gross, 1995)] and many others. The resistor represents the power loss described earlier, while the inductor accounts for the inductance produced due to circulating eddy currents. The dynamic circuit model is given in Figure 7.

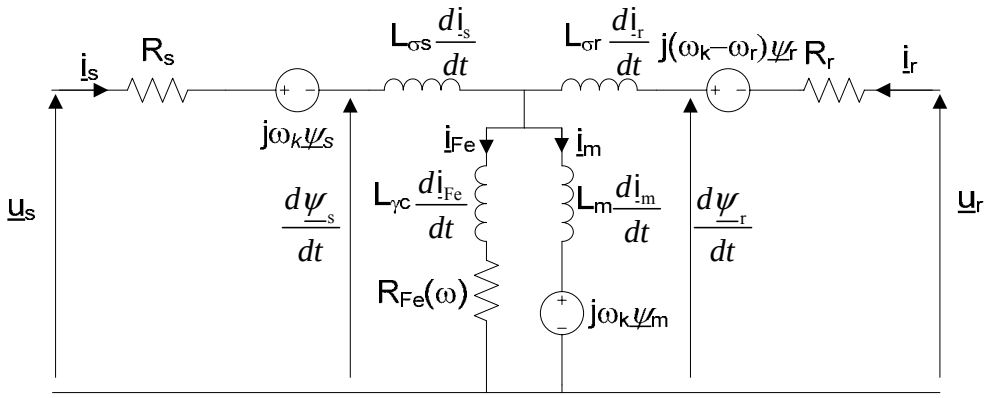

Figure 7: Dynamic Circuit Model of an Induction Machine, with Core Loss Branch

Note that in the above mode, the frequency used for the core loss resistance is the supply frequency. The space-vector model for the stator reference frame for the above circuit then becomes

$$\underline{u}_s = R_s \underline{i}_s + \frac{d\underline{\psi}_s}{dt} \tag{38}$$

$$0 = R_r \underline{i}_r + \frac{d\underline{\psi}_r}{dt} - j\omega\underline{\psi}_r \tag{39}$$

$$R_{Fe}(\omega)\underline{i}_{Fe} + L_{\gamma c}\frac{d\underline{i}_{Fe}}{dt} = \frac{d\underline{\psi}_m}{dt} \tag{40}$$

$$\underline{i}_m + \underline{i}_{Fe} = \underline{i}_s + \underline{i}_r \tag{41}$$

$$\underline{\psi}_s = L_{\sigma s}\underline{i}_s + \underline{\psi}_m \tag{42}$$

$$\underline{\psi}_r = L_{\sigma r}\underline{i}_r + \underline{\psi}_m \tag{43}$$

$$\underline{\psi}_m = L_m \underline{i}_m \tag{44}$$

The steady-state equivalent circuit is going to be useful for the purposes of this thesis and as such, is shown in Figure 8.

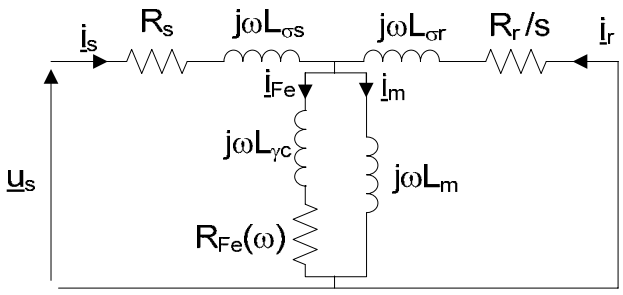

Figure 8: Steady-State Circuit Model of an Induction Machine, with Core Loss Branch

Note that the eddy current inductance has been repeatedly reported to be negligible in the case of sinusoidal and non-sinusoidal supplies [(Honsinger, 1980); (Sousa et al., 1992); (Levi et al., 1995) & (Levi et al., 2005)]. As such, it is henceforth ignored.

3.9 DC Step Voltage Test

The step voltage response at standstill is determined by setting the rotor speed to zero in the dynamic model described in equations (4) to (7). The equivalent circuit corresponding to this case is given in the figure below.

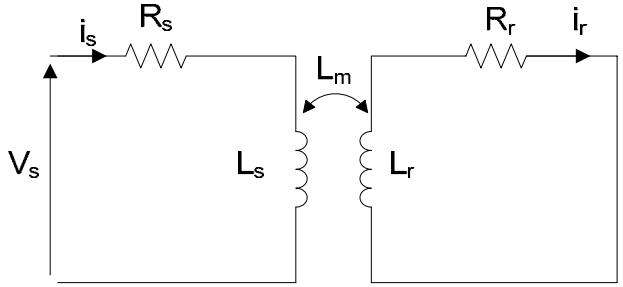

Figure 9: Induction Machine Circuit at Standstill (Belloc et. al, 2006)

Zeveke & Lonkin (1975) determined that the stator current response (reprinted in Belloc et al., 2006) for the circuit in Figure 9 is

$$i_s(t) = \frac{V_s}{R_s}\left[1 + p_2 \frac{1 + p_1 T_r}{p_1 - p_2} e^{p_1 t} - p_1 \frac{1 + p_2 T_r}{p_1 - p_2} e^{p_2 t}\right] \tag{45}$$

where

$$p_{1,2} = -\frac{1}{2\left(1-k^2\right)}\left[\frac{1}{T_s} + \frac{1}{T_r} \mp \sqrt{\left(\frac{1}{T_s} + \frac{1}{T_r}\right)^2 - 4\frac{\left(1-k^2\right)}{T_s T_r}}\right], \tag{46}$$

$$T_s = \frac{L_s}{R_s}, T_r = \frac{L_r}{R_r}, k = \frac{L_m}{\sqrt{L_s L_r}} \tag{47}$$

The machine parameters are determined by using the dynamic model equations, from which the following relationship between stator current and applied voltage is derived:

$$\begin{aligned} 0 &= \frac{R_r}{L_r}t + 1 - \frac{R_s R_r}{L_r V_s}\left[\int i_s dt\right] - \frac{R_r L_s + L_r R_s}{L_r V_s} i_s + \frac{L_m^2 - L_r L_s}{L_r V_s}\left[\frac{di_s}{dt}\right] \\ &= At + 1 + B\left[\int i_s dt\right] + Ci_s + D\left[\frac{di_s}{dt}\right] \end{aligned} \tag{48}$$

If the current is read at four sample times, a system of equations with five unknowns is produced via the above equation. The system is then solved and the coefficients (A, B, C and D) are determined. With these values known, the following can be calculated (Belloc et al., 2006).

$$R_s = \frac{-BV_s}{A},\ L_s = -\frac{CV_s + R_s}{A}, T_s = \frac{L_s}{R_s}, T_r = \frac{1}{A}, k = \sqrt{\frac{DV_s}{L_s} + 1} \tag{49}$$

One interesting thing to note here is that if the stator resistance is chosen to be the known value, the system defined by (48) does not have a unique analytical solution. However, if the rotor leakage reactance is tied to the stator reactance, the above produces a solvable system. The method can then be used to determine remaining standard circuit parameters as follows.

$$R_r = AL_r \tag{50}$$

$$L_m = \sqrt{DL_r V_s + L_r L_s} \tag{51}$$

It should be noted that a method was determined to allow both stator and rotor leakage inductances to be determined analytically. It is outlined in Chapter 4.

The time derivative and integral of the current in (45) is given below (Belloc et al., 2006).

$$\frac{di_s(t)}{dt} = \frac{V_s p_1 p_2}{R_s(p_1 - p_2)}\left[(1 + p_1 T_r)e^{p_1 t} - (1 + p_2 T_r)e^{p_2 t}\right] \tag{52}$$

$$\int i_s(t)dt = \frac{V_s}{R_s}\left[t + \frac{p_2(1 + p_1 T_r)}{p_1(p_1 - p_2)}\left(e^{p_1 t} - 1\right) - \frac{p_1(1 + p_2 T_r)}{p_1(p_1 - p_2)}\left(e^{p_2 t} - 1\right)\right] \tag{53}$$

However, it is clear that using (52) and (53) in (48) will prove unwieldy. It is therefore suggested to use initial values by obtaining the approximate area under the current curve (using the trapezoid method) and the approximate slope of the current (using the previous sample point). The initial solutions for the parameters are calculated, allowing the derivative and integral of the current to be calculated using (52) and (53). The solution for the system is recalculated and the iterations continue until convergence is reached.

Chapter 4
Author's Contributions

This section contains the ideas, concepts and equations (with their derivations) not found in the literature and determined by the author. Chapter 5 provides the results of these ideas.

4.1 Small-signal Model with Core Losses

Utilising the tools cultivated by Repo, the author developed a similar small-signal model for an induction machine with core losses included. The model was derived from the dynamic model given in (38) to (44). The derivation is outlined here.

The following system of equations is produced from the dynamic model with a frequency-dependent core loss resistor.

$$\underline{u}_{\mathrm{s}0} + \Delta\underline{u}_{\mathrm{s}} = R_{\mathrm{s}}\left(\underline{i}_{\mathrm{s}0} + \Delta\underline{i}_{\mathrm{s}}\right) + \frac{d}{dt}\left[L_{\sigma\mathrm{s}}\left(\underline{i}_{\mathrm{s}0} + \Delta\underline{i}_{\mathrm{s}}\right) + L_{\mathrm{m}}\left(\underline{i}_{\mathrm{m}0} + \Delta\underline{i}_{\mathrm{m}}\right)\right] \tag{54}$$

$$\begin{aligned} 0 = {} & R_{\mathrm{r}}\left(\underline{i}_{\mathrm{r}0} + \Delta\underline{i}_{\mathrm{r}}\right) + \frac{d}{dt}\left[L_{\sigma\mathrm{r}}\left(\underline{i}_{\mathrm{r}0} + \Delta\underline{i}_{\mathrm{r}}\right) + L_{\mathrm{m}}\left(\underline{i}_{\mathrm{m}0} + \Delta\underline{i}_{\mathrm{m}}\right)\right] \\ & -\mathrm{j}\left(\omega_{\mathrm{r}0} + \Delta\omega_{\mathrm{r}}\right)\left[L_{\sigma\mathrm{r}}\left(\underline{i}_{\mathrm{r}0} + \Delta\underline{i}_{\mathrm{r}}\right) + L_{\mathrm{m}}\left(\underline{i}_{\mathrm{m}0} + \Delta\underline{i}_{\mathrm{m}}\right)\right] \end{aligned} \tag{55}$$

$$\left(R_{\mathrm{Fe}}\left(\omega_{\mathrm{l}}\right)\underline{i}_{\mathrm{Fe}0} + R_{\mathrm{Fe}}\left(\omega\right)\Delta\underline{i}_{\mathrm{Fe}}\right) + L_{\gamma\mathrm{c}}\frac{d}{dt}\left(\underline{i}_{\mathrm{Fe}0} + \Delta\underline{i}_{\mathrm{Fe}}\right) = L_{\mathrm{m}}\frac{d}{dt}\left(\underline{i}_{\mathrm{m}0} + \Delta\underline{i}_{\mathrm{m}}\right) \tag{56}$$

where

x_{x0} values represent steady-state values
ω_{l} is the fundamental of the applied voltage
ω is the angular speed of the electrical frequency under consideration

Note that in (56), the steady-state (or fundamental) current experience the core loss resistance at the fundamental supply frequency. The voltage impulse excites a wide range of frequencies and so produces current at these frequencies. If the model included saturation and skin effects, it need not be considered linearised around the rated frequency point and the steady-state voltage values $\left(\text{i.e. } Ri, L\frac{di}{dt}\right)$ could be subtracted from (56). The core loss resistance experienced by $\Delta\underline{i}_{Fe}$ and used in the final models will be defined in the following sections.

However, the small-signal model is linearised around the rated operating point, at the rated frequency. Presently, an approximation is made, allowing this resistance to equal the value seen by the steady-state current. As will be seen, the following approximation is valid since the effect of this resistance on the small-signal model is not significant.

$$\left(R_{\mathrm{Fe}}\left(\omega_{\mathrm{l}}\right)\underline{i}_{\mathrm{Fe0}}+R_{\mathrm{Fe}}\left(\omega_{\mathrm{l}}\right)\Delta\underline{i}_{\mathrm{Fe}}\right)+L_{\gamma\mathrm{c}}\frac{d}{dt}\left(\underline{i}_{\mathrm{Fe0}}+\Delta\underline{i}_{\mathrm{Fe}}\right)\approx L_{\mathrm{m}}\frac{d}{dt}\left(\underline{i}_{\mathrm{m0}}+\Delta\underline{i}_{\mathrm{m}}\right) \tag{57}$$

Subtracting the steady-state values from (54), (55) and (57), and assuming no change in the mechanical speed of the rotor,

$$\Delta\underline{u}_{\mathrm{s}}=R_{\mathrm{s}}\Delta\underline{i}_{\mathrm{s}}+\frac{d}{dt}\left(L_{\sigma\mathrm{s}}\Delta\underline{i}_{\mathrm{s}}+L_{\mathrm{m}}\Delta\underline{i}_{\mathrm{m}}\right) \tag{58}$$

$$0=R_{\mathrm{r}}\Delta\underline{i}_{\mathrm{r}}+\frac{d}{dt}\left(L_{\sigma\mathrm{r}}\Delta\underline{i}_{\mathrm{r}}+L_{\mathrm{m}}\Delta\underline{i}_{\mathrm{m}}\right)-\mathrm{j}\omega_{\mathrm{r0}}\left(L_{\sigma\mathrm{r}}\Delta\underline{i}_{\mathrm{r}}+L_{\mathrm{m}}\Delta\underline{i}_{\mathrm{m}}\right) \tag{59}$$

$$R_{\mathrm{Fe}}\left(\omega_{\mathrm{l}}\right)\Delta\underline{i}_{\mathrm{Fe}}+L_{\gamma\mathrm{c}}\frac{d\Delta\underline{i}_{\mathrm{Fe}}}{dt}=L_{\mathrm{m}}\frac{d}{dt}\Delta\underline{i}_{\mathrm{m}} \tag{60}$$

The current relationship is maintained in the small-signal model

$$\Delta\underline{i}_{\mathrm{m}}+\Delta\underline{i}_{\mathrm{Fe}}=\Delta\underline{i}_{\mathrm{s}}+\Delta\underline{i}_{\mathrm{r}}\Rightarrow\Delta\underline{i}_{\mathrm{m}}=\Delta\underline{i}_{\mathrm{s}}+\Delta\underline{i}_{\mathrm{r}}-\Delta\underline{i}_{\mathrm{Fe}} \tag{61}$$

Therefore

$$R_{Fe}\left(\omega_{\mathrm{l}}\right)\Delta\underline{i}_{\mathrm{Fe}}+L_{\gamma\mathrm{c}}\frac{d\Delta\underline{i}_{\mathrm{Fe}}}{dt}=L_{\mathrm{m}}\frac{d}{dt}\left(\Delta\underline{i}_{\mathrm{s}}+\Delta\underline{i}_{\mathrm{r}}-\Delta\underline{i}_{\mathrm{Fe}}\right) \tag{62}$$

In the frequency domain, (58), (59) and (62) become (using Laplace transforms)

$$\Delta \underline{u}_{\mathrm{s}} = R_{\mathrm{s}} \Delta \underline{i}_{\mathrm{s}} + \mathrm{j}\omega \left(L_{\sigma \mathrm{s}} \Delta \underline{i}_{\mathrm{s}} + L_{\mathrm{m}} \Delta \underline{i}_{\mathrm{m}} \right) \tag{63}$$

$$0 = R_{\mathrm{r}} \Delta \underline{i}_{\mathrm{r}} + \mathrm{j}\omega \left(L_{\sigma \mathrm{r}} \Delta \underline{i}_{\mathrm{r}} + L_{\mathrm{m}} \Delta \underline{i}_{\mathrm{m}} \right) - \mathrm{j}\omega_{\mathrm{r0}} \left(L_{\sigma \mathrm{r}} \Delta \underline{i}_{\mathrm{r}} + L_{\mathrm{m}} \Delta \underline{i}_{\mathrm{m}} \right) \tag{64}$$

$$R_{\mathrm{Fe}} \left(\omega_{\mathrm{l}} \right) \Delta \underline{i}_{\mathrm{Fe}} + \mathrm{j}\omega L_{\gamma \mathrm{c}} \Delta \underline{i}_{\mathrm{Fe}} = \mathrm{j}\omega L_{\mathrm{m}} \left(\Delta \underline{i}_{\mathrm{s}} + \Delta \underline{i}_{\mathrm{r}} \right) - \mathrm{j}\omega L_{\mathrm{m}} \Delta \underline{i}_{\mathrm{Fe}} \tag{65}$$

Rearranging,

$$\Delta \underline{i}_{\mathrm{Fe}} = \frac{\mathrm{j}\omega L_{\mathrm{m}} \left(\Delta \underline{i}_{\mathrm{s}} + \Delta \underline{i}_{\mathrm{r}} \right)}{\left(R_{\mathrm{Fe}} \left(\omega_{\mathrm{l}} \right) + \mathrm{j}\omega L_{\gamma \mathrm{c}} + \mathrm{j}\omega L_{\mathrm{m}} \right)} \tag{66}$$

Inserting (66) into (61),

$$\begin{aligned} \Delta \underline{i}_{\mathrm{m}} &= \Delta \underline{i}_{\mathrm{s}} + \Delta \underline{i}_{\mathrm{r}} - \frac{\mathrm{j}\omega L_{\mathrm{m}} \left(\Delta \underline{i}_{\mathrm{s}} + \Delta \underline{i}_{\mathrm{r}} \right)}{\left(R_{\mathrm{Fe}} \left(\omega_{\mathrm{l}} \right) + \mathrm{j}\omega L_{\gamma \mathrm{c}} + \mathrm{j}\omega L_{\mathrm{m}} \right)} \\ &= \left(\Delta \underline{i}_{\mathrm{s}} + \Delta \underline{i}_{\mathrm{r}} \right) \left[1 - \frac{\mathrm{j}\omega L_{\mathrm{m}}}{\left(R_{\mathrm{Fe}} \left(\omega_{\mathrm{l}} \right) + \mathrm{j}\omega L_{\gamma \mathrm{c}} + \mathrm{j}\omega L_{\mathrm{m}} \right)} \right] \end{aligned} \tag{67}$$

Inserting (67) into (64),

$$\begin{aligned} 0 = {} & R_{\mathrm{r}} \Delta \underline{i}_{\mathrm{r}} + \mathrm{j}\omega L_{\sigma \mathrm{r}} \Delta \underline{i}_{\mathrm{r}} + \mathrm{j}\omega L_{\mathrm{m}} \Delta \underline{i}_{\mathrm{s}} + \mathrm{j}\omega L_{\mathrm{m}} \Delta \underline{i}_{\mathrm{r}} - \mathrm{j}\omega L_{\mathrm{m}} \frac{\mathrm{j}\omega L_{\mathrm{m}} \left(\Delta \underline{i}_{\mathrm{s}} + \Delta \underline{i}_{\mathrm{r}} \right)}{\left(R_{\mathrm{Fe}} \left(\omega_{\mathrm{l}} \right) + \mathrm{j}\omega L_{\gamma \mathrm{c}} + \mathrm{j}\omega L_{\mathrm{m}} \right)} \\ & - \mathrm{j}\omega_{\mathrm{r0}} L_{\sigma \mathrm{r}} \Delta \underline{i}_{\mathrm{r}} - \mathrm{j}\omega_{\mathrm{r0}} L_{\mathrm{m}} \Delta \underline{i}_{\mathrm{s}} - \mathrm{j}\omega_{\mathrm{r0}} L_{\mathrm{m}} \Delta \underline{i}_{\mathrm{r}} + \mathrm{j}\omega_{\mathrm{r0}} L_{\mathrm{m}} \frac{\mathrm{j}\omega L_{m} \left(\Delta \underline{i}_{s} + \Delta \underline{i}_{r} \right)}{\left(R_{\mathrm{Fe}} \left(\omega_{\mathrm{l}} \right) + \mathrm{j}\omega L_{\gamma \mathrm{c}} + \mathrm{j}\omega L_{\mathrm{m}} \right)} \end{aligned} \tag{68}$$

Rearranging,

$$\Delta \underline{i}_{\mathrm{r}} = -\Delta \underline{i}_{\mathrm{s}} \frac{\left[\mathrm{j}(\omega - \omega_{\mathrm{r0}}) L_{\mathrm{m}} + (\omega - \omega_{\mathrm{r0}}) \frac{\omega {L_{\mathrm{m}}}^2}{\left(R_{\mathrm{Fe}} \left(\omega_{\mathrm{s0}} \right) + j\omega L_{\gamma \mathrm{c}} + j\omega L_{\mathrm{m}} \right)} \right]}{\left[R_{\mathrm{r}} + \mathrm{j}(\omega - \omega_{\mathrm{r0}}) L_{\sigma \mathrm{r}} + \mathrm{j}(\omega - \omega_{\mathrm{r0}}) L_{\mathrm{m}} + (\omega - \omega_{\mathrm{r0}}) \frac{\omega {L_{\mathrm{m}}}^2}{\left(R_{\mathrm{Fe}} \left(\omega_{\mathrm{l}} \right) + j\omega L_{\gamma \mathrm{c}} + j\omega L_{\mathrm{m}} \right)} \right]} \tag{69}$$

Inserting (69) into (67)

$$\Delta \underline{i}_{\mathrm{m}} = \Delta \underline{i}_{\mathrm{s}} \left(1 - \frac{\left[\mathrm{j}(\omega - \omega_{\mathrm{r0}}) L_{\mathrm{m}} + (\omega - \omega_{\mathrm{r0}}) \dfrac{\omega L_{\mathrm{m}}{}^2}{\left(R_{\mathrm{Fe}}(\omega_{\mathrm{l}}) + j\omega L_{\gamma \mathrm{c}} + j\omega L_{\mathrm{m}} \right)} \right]}{\left[\begin{array}{l} R_r + \mathrm{j}(\omega - \omega_{\mathrm{r0}}) L_{\sigma \mathrm{r}} + \mathrm{j}(\omega - \omega_{r0}) L_{\mathrm{m}} \\ \qquad + (\omega - \omega_{\mathrm{r0}}) \dfrac{\omega L_{\mathrm{m}}{}^2}{\left(R_{\mathrm{Fe}}(\omega_{\mathrm{l}}) + \mathrm{j}\omega L_{\gamma \mathrm{c}} + \mathrm{j}\omega L_{\mathrm{m}} \right)} \end{array} \right]} \right) \left(1 - \frac{\mathrm{j}\omega L_{\mathrm{m}}}{\left(R_{\mathrm{Fe}}(\omega_{\mathrm{l}}) + \mathrm{j}\omega L_{\gamma \mathrm{c}} + \mathrm{j}\omega L_{\mathrm{m}} \right)} \right) \tag{70}$$

Inserting (70) into (63) and rearranging,

$$\frac{\Delta \underline{u}_{\mathrm{s}}}{\Delta \underline{i}_{\mathrm{s}}} = \left[\begin{array}{l} R_{\mathrm{s}} + \mathrm{j}\omega L_{\sigma \mathrm{s}} \\ \qquad + (\mathrm{j}\omega L_{\mathrm{m}} + \omega \underline{z}_{\mathrm{l}}) \left(1 - \dfrac{\left[\mathrm{j}(\omega - \omega_{\mathrm{r0}}) L_m + (\omega - \omega_{\mathrm{r0}}) \underline{z}_{\mathrm{l}} \right]}{\left[R_{\mathrm{r}} + \mathrm{j}(\omega - \omega_{\mathrm{r0}}) L_{\sigma \mathrm{r}} + \mathrm{j}(\omega - \omega_{\mathrm{r0}}) L_{\mathrm{m}} + (\omega - \omega_{\mathrm{r0}}) \underline{z}_{\mathrm{l}} \right]} \right) \end{array} \right] \tag{72}$$

where

$$\underline{z}_{\mathrm{l}} = \frac{\omega L_{\mathrm{m}}{}^2}{\left(R_{\mathrm{Fe}}(\omega_{\mathrm{l}}) + \mathrm{j}\omega L_{\gamma \mathrm{c}} + \mathrm{j}\omega L_{\mathrm{m}} \right)} \tag{73}$$

The admittance in the frequency domain is then obtained by calculating the inverse of the above at all frequencies of interest. Note that the eddy current leakage inductance has been left in the model for future applications (e.g. placing all frequency-dependent core loss behaviour in this circuit element).

At this point, a problem was encountered in the thesis. The search algorithm was to compare the core losses calculated by Dlala's FE model to the calculated power losses across the core loss resistance and determine parameters by minimising the error. To calculate P_c, one needs to know either the current through the core loss branch or the air-gap voltage. It is possible to try and determine all parameters from the search algorithm simultaneously. However, this approach was unfeasible as the search algorithm does not converge.

The following section provides a workaround for the problem.

4.2 Algorithms to Determine Core Loss Parameters (Fixed Steinmetz Coefficient)

The author hypothesised that the solution space for the algorithm may be too large. To address this issue, a series of iterations with specified constraints were implemented.

The standard small-signal model, with core losses ignored, was known to converge to reasonable parameters. Therefore, the author first decided to use the standard model to find the initial approximations

$$\boldsymbol{\theta}'_{\mathrm{m}} = \left\{ R'_{\mathrm{r}}, L'_{\sigma\mathrm{s}}, L'_{\mathrm{m}} \right\} \tag{74}$$

where

R'_{r} is the approximate rotor resistance
$L'_{\sigma\mathrm{s}}$ is the approximate stator leakage reactance
L'_{m} is the approximate magnetising reactance

The cost function used to minimise the error for the above solution vector was

$$X_{Zi} = \frac{\mathrm{Re}\left\{ Y_{\mathrm{m}i} - Y_{ci} \right\}^2 + \mathrm{Im}\left\{ Y_{\mathrm{m}i} - Y_{ci} \right\}^2}{\mathrm{Re}\left\{ Y_{\mathrm{m}i} \right\}^2 + \mathrm{Im}\left\{ Y_{\mathrm{m}i} \right\}^2}, \overline{X}_Z = \frac{\sum_{i=1}^{N} X_{Zi}}{N} \tag{75}$$

$$I = \frac{1}{2}\left[\overline{X_Z} + \sigma\left(X_Z \right) \right], \tag{76}$$

where

Y_{ci} is the admittance calculated analytically for the *i*th frequency
$Y_{\mathrm{m}i}$ is the "measured" admittance for the *i*th frequency
$\sigma\left(X_Z \right)$ is the standard deviation of X_Z

The standard deviation was used to give some significance to the “shape” of the curve. If the test/calculated ratio could be kept somewhat constant, it may point towards an unconsidered aspect.

The approximate solution vector was then used to find an approximation for the core loss parameters using the core loss steady-state equivalent circuit in Figure 8.

$$\boldsymbol{\theta}'_{\mathrm{k}} = \left\{ k'_{\mathrm{ch}}, k'_{\mathrm{e}} \right\} \tag{77}$$

where

$k_{ch}^{'}$ is the approximate hysteresis coefficient (times core loss coefficient)

$k_{ce}^{'}$ is the approximate eddy-current coefficient (times core loss coefficient)

The cost function used for this approximation was

$$X_{Pi} = \frac{\left|P_{mi}^2 - P_{ci}^2\right|}{P_{mi}^2}, \overline{X}_P = \frac{\sum_{i=1}^{N} X_{Pi}}{N} \tag{78}$$

$$I = \frac{1}{2}\left[\overline{X_P} + \sigma\left(X_P\right)\right] \tag{79}$$

where

P_{ci} is the core loss calculated analytically for the *i*th frequency and voltage point

P_{mi} is the core loss calculated by the FEA for the *i*th frequency and voltage point

$\sigma\left(X_P\right)$ is the standard deviation of X_P

These first approximations were used to reduce the solution space in all dimensions. The lower limits for the parameters were set to $\left\{\theta_m', \theta_k'\right\} \times 10^{-2}$ and the upper limits were set to $\left\{\theta_m', \theta_k'\right\} \times 10^{2}$, thereby allowing a four magnitude solution space in each dimension of the solution vector.

Finally, the small-signal model, based on Figure 7 (with core losses included) and the steady-state model of Figure 8 (with core losses included) were used together to refine the approximations.

The cost function used for the algorithm was

$$I = \frac{1}{2}\left[\overline{X_Z} + \sigma\left(X_Z\right)\right] + \frac{1}{2}\left[\overline{X_P} + \sigma\left(X_P\right)\right] \tag{80}$$

The solution then converged and the process was considered a success. The convergence is shown in Table 10 in page 60.

4.3 Core Loss Resistance Model with a Variable Steinmetz Coefficient

During the course of the thesis, it was discovered that leaving the Steinmetz coefficient set at 2 (as in (20)) was unsatisfactory. It was therefore desirable to allow this constant to

become a variable parameter, optimised by the search algorithm. The resistance for the core loss must be defined with these conditions in mind. The derivation is outlined here.

Let the Steinmetz coefficient be an unknown parameter between, say, 1 and 6. The core power loss equation then becomes

$$P_{\mathrm{c}} = k_{\mathrm{h}}\left(1+s\right) f \phi^{n} + k_{\mathrm{e}}\left(1+s^{2}\right) f^{2}\phi^{2} \tag{81}$$

Using (22) and (23),

$$P_{\mathrm{c}} = k_{\mathrm{h}}\left(1+s\right)\frac{\omega}{2\pi}\left(\sqrt{k_{\mathrm{c}}}\frac{V_{\mathrm{m}}}{\omega}\right)^{n} + k_{\mathrm{e}}\left(1+s^{2}\right)\left(\frac{\omega}{2\pi}\right)^{2}\left(\sqrt{k_{\mathrm{c}}}\frac{V_{\mathrm{m}}}{\omega}\right)^{2} = \frac{{V_{\mathrm{m}}}^{2}}{R_{\mathrm{Fe}}} \tag{82}$$

or,

$$\frac{{V_{\mathrm{m}}}^{2}}{R_{\mathrm{Fe}}} = \frac{k_{\mathrm{c}}k_{\mathrm{h}}}{2\pi}\left(1+s\right)\frac{{V_{\mathrm{m}}}^{2}}{\omega}\left(\frac{V_{\mathrm{m}}}{\omega}\right)^{n-2} + \frac{k_{\mathrm{c}}k_{\mathrm{e}}}{4\pi^{2}}\left(1+s^{2}\right){V_{\mathrm{m}}}^{2} \tag{83}$$

Dividing (83) by ${V_m}^2$

$$\frac{1}{R_{\mathrm{Fe}}} = \frac{k_{\mathrm{c}}k_{\mathrm{h}}}{2\pi}\frac{\left(1+s\right)}{\omega}\left(\frac{V_{\mathrm{m}}}{\omega}\right)^{n-2} + \frac{k_{\mathrm{c}}k_{\mathrm{e}}}{4\pi^{2}}\left(1+s^{2}\right) \tag{84}$$

$$R_{\mathrm{Fe}} = \left[k_{\mathrm{ch}}\frac{\left(1+s\right)}{\left|\omega\right|}\left|\frac{V_{\mathrm{m}}}{\omega}\right|^{n-2} + k_{\mathrm{ce}}\left(1+s^{2}\right)\right]^{-1} \tag{85}$$

where

$$k_{\mathrm{ch}} = \frac{k_{\mathrm{c}}k_{\mathrm{h}}}{2\pi}, k_{\mathrm{ce}} = \frac{k_{\mathrm{c}}k_{\mathrm{e}}}{4\pi^{2}} \tag{86}$$

Note here that absolute values of frequencies are used as random values of the Steinmetz coefficient may produce complex numbers with negative frequencies. In (85), the air-gap voltage needs to be calculated to evaluate the core loss resistance. However, this resistance is required to calculate the stator current and therefore, the air-gap voltage.

Another workaround, similar to the one outlined in the last section, is presented in the following section.

4.4 Algorithms to Determine Core Loss Parameters (Variable Steinmetz Coefficient)

Section 4.2 outlines a method to obtain the circuit parameters for Figure 7 if the Steinmetz coefficient is fixed. For the variable Steinmetz coefficient, however, V_{m} needs to be calculated to evaluate R_{Fe} itself. Furthermore, to calculate V_{m}, the stator current (and therefore R_{Fe}) needs to be known. A circular problem is encountered. Fixed-point iteration methods tend to resolve such problems given that the criteria for convergence are met, one of which is a reasonable initial guess.

The steady-state circuit of Figure 3 can be used to calculate an initial guess for the air-gap voltage V_{m_0} from the approximate parameters calculated using the small-signal model, without core losses. For the given test core loss parameter vector $\left(\boldsymbol{\theta}_{\mathrm{k}i} = \{k_{\mathrm{ch}i}, k_{\mathrm{ce}i}, n_i\}\right)$, the following sequence is generated with an approximate machine parameter vector $\left(\boldsymbol{\theta}'_{\mathrm{m}_0} = \left\{R'_{\mathrm{r}}, L'_{\sigma\mathrm{s}}, L'_{\mathrm{m}}\right\}\right)$.

The initial air-gap voltage (based on Figure 3) is

$$V_{\mathrm{m}_0} = f_{\mathrm{std}}\left(\boldsymbol{\theta}'_{\mathrm{m}_0}\right) \tag{87}$$

where

f_{std} is the air-gap voltage function of the steady-state circuit, without core losses

An initial core loss resistance is then calculated based on this voltage and the test core loss parameter vector using (85).

$$R_{\mathrm{Fe}_0} = f\left(V_{\mathrm{m}_0}, \boldsymbol{\theta}_{\mathrm{k}i}\right) \tag{88}$$

A new machine parameter vector is formed, with the core loss resistance included.

$$\boldsymbol{\theta}_{\mathrm{m}_0} = \left\{R'_{\mathrm{r}}, L'_{\sigma\mathrm{s}}, L'_{\mathrm{m}}, R_{\mathrm{Fe}_0}\right\} \tag{89}$$

The air-gap voltage is then calculated, using the steady-state model of Figure 8 with the above parameter vector and the test core loss parameter vector. The following iteration is repeated until convergence is reached.

$$V_{\mathrm{m}_{n+1}} = f_{\mathrm{cl}}\left(\boldsymbol{\theta}_{\mathrm{m}_n}, \boldsymbol{\theta}_{\mathrm{k}i}\right) \tag{90}$$

$$R_{\mathrm{Fe}_{n+1}} = f\left(V_{\mathrm{m}_{n+1}}, \boldsymbol{\theta}_{\mathrm{k}i}\right) \tag{91}$$

$$\boldsymbol{\theta}_{\mathrm{m}_{n+1}} = \left\{R_{\mathrm{r}}^{'}, L_{\sigma\mathrm{s}}^{'}, L_{\mathrm{m}}^{'}, R_{\mathrm{Fe}_{n+1}}\right\} \tag{92}$$

where

f_{cl} is the air-gap voltage function of the steady-state circuit, with core losses

f is the function defined in (85)

It should be noted that the above usually converges in 3 to 8 iterations. However, 25 iterations have also been observed. By the end of these iterations, the algorithm has initial approximations for all the required parameters

$$\boldsymbol{\theta}' = \left\{R_{\mathrm{r}}^{'}, L_{\sigma\mathrm{s}}^{'}, L_{\mathrm{m}}^{'}, k_{\mathrm{h}}^{'}, k_{\mathrm{e}}^{'}, n^{'}\right\}$$

As in Section 4.2, a refinement of the parameters is obtained by restricting the solution space for the system and repeating the search using the steady-steady and small-signal models, based on Figure 8 and Figure 7.

For the first five parameters, the upper and lower limits are restricted as before. However, for *m*, the upper limit is chosen to be $n^{'} \times 10^{1}$ and the lower limit is $n^{'} \times 10^{-1}$.

4.5 Combined Method to Determine Leakage Inductances Independently

As discussed in Chapter 1, the aim of the project is to determine circuit parameters experimentally, without the use of FEA. Although the ratio of stator-to-rotor leakage inductance can be approximated (based on machine type and geometry as in IEEE Standard 112), it is preferred to be able to calculate them independently for a given machine. Previously, this ratio had been obtained using the impedance method via FEA. However, this section presents a Combined Method, based on the results of the DC step voltage test and impulse response test, which allows the stator and rotor leakage inductances to be determined independently.

Without relating the stator and rotor leakage inductances, the parameters given in (49) can be obtained. Specifically, the rotor time constant and the coupling coefficient are known. These parameters give a sense of the relationship between stator and rotor quantities and may therefore be used to relate these values. If these parameters are

considered a close approximation to values during operating conditions, the magnetising inductance and rotor leakage inductance for a given test vector (containing rotor resistance and stator leakage inductance) can be determined without increasing the order of the system as follows.

$$L_{\mathrm{r}} = T_{\mathrm{r}} R_{ri} \tag{93}$$

$$L_{\mathrm{m}} = \frac{k^2 L_{\mathrm{r}} + \sqrt{k^4 L_{\mathrm{r}}^2 + 4k^2 L_{\mathrm{r}} L_{\sigma si}}}{2} \tag{94}$$

$$L_{\sigma \mathrm{r}} = L_{\mathrm{r}} - L_{\mathrm{m}} \tag{95}$$

where

R_{ri} is the test rotor resistance value
$L_{\sigma si}$ is the test stator leakage inductance value

Note that the positive square root is chosen in (94) to provide the positive magnetising inductance. For the approximate machines parameters (as per Section 4.2 and Section 4.4), the stator inductance determined from the step voltage test can be used directly and (94) reduces to

$$L_{\mathrm{m}} = k\sqrt{L_{\mathrm{r}} L_{\mathrm{s}}} \tag{96}$$

In this case, the DE algorithm is required to search along the dimension of just the rotor resistance.

Chapter 5

Results

5.1 Parameters for Standard Small-Signal Model using Impulse Response Tests

The voltage impulse described by (11) was applied to a single cage induction machine with the following characteristics:

Table 2: Characteristics of the 37kW Induction Machine

Type	Star	Frequency (Hz)	50
Rated Power (kW)	37	R_s (Ω)	0.0836
Rated Voltage (V)	380	R_r (Ω)	0.0656
Poles	4	$L_{\sigma s}$ (mH)	0.749
Full Load Speed (rpm)	1470	L_m (mH)	26.3
Synch. Speed (rpm)	1500	$L_{\sigma r}$ (mH)	1.50

The parameters for the voltage impulse where chosen to be $f_d = 100$ Hz, $t_{st} = 0.1$ s, $t_d = 0.005$ s, $a_{rel} = 0.15$, $|\underline{u}_s| = 310.27$ V

$|\underline{u}_s|$ is calculated based on the definition of a space-vector as follows.

$$|\underline{u}_s| = \left| \frac{2}{3} \left[u_{sa}(t) + \underline{a} u_{sb}(t) + \underline{a}^2 u_{sc}(t) \right] \right| \tag{97}$$

$$u_{sa}(t) = \hat{u}_\varphi \cos(\omega t + \varphi) \tag{98}$$

$$u_{sb}(t) = \hat{u}_\varphi \cos\left(\omega t + \varphi + \frac{2\pi}{3} \right) \tag{99}$$

$$u_{sc}(t) = \hat{u}_{\varphi} \cos\left(\omega t + \varphi + \frac{4\pi}{3}\right) \tag{100}$$

$$\text{letting } t = 0, \varphi = 0, \underline{a} = e^{j\frac{2}{3}\pi}, \hat{u}_{\varphi} = \sqrt{\frac{2}{3}} U_{llrms} \tag{101}$$

$$\left|\underline{u}_s\right| = \frac{2}{3}\hat{u}_{\varphi}\left|1 - \frac{1}{2}e^{j\frac{2\pi}{3}} - \frac{1}{2}e^{j\frac{4\pi}{3}}\right| = 310.27 \text{ V} \tag{102}$$

The frequency response of the voltage impulse, presented in Section 3.4, its current and admittance response, as obtained from the small-signal model presented in Section 3.5, are given in the following figures.

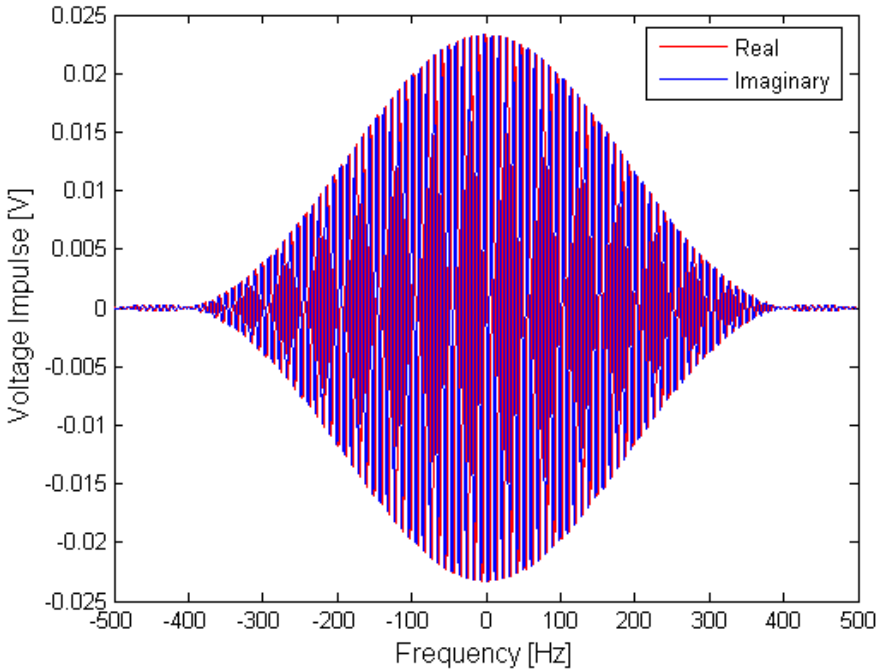

Figure 10: Voltage Impulse in Frequency Domain

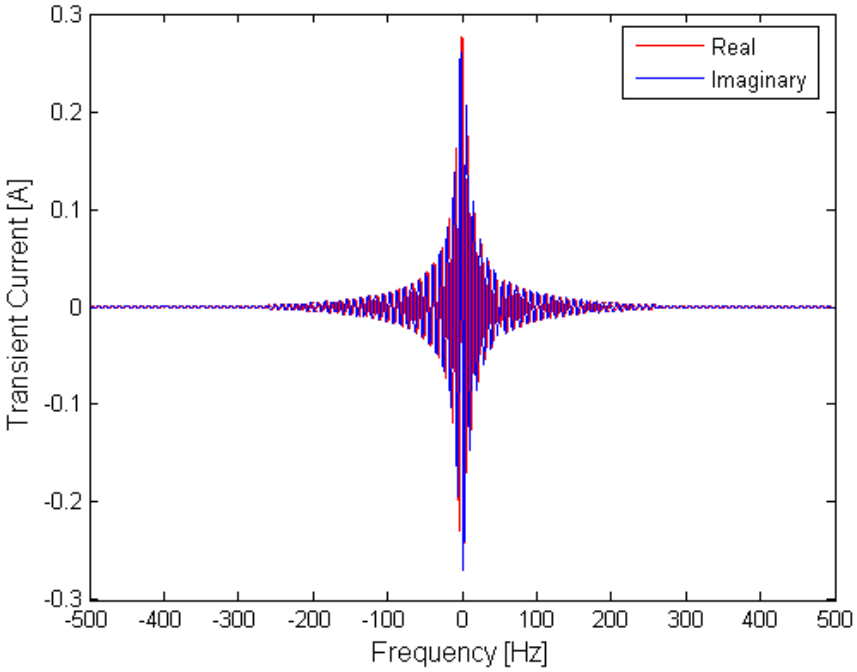

Figure 11: Current Response to Voltage Impulse in Frequency Domain

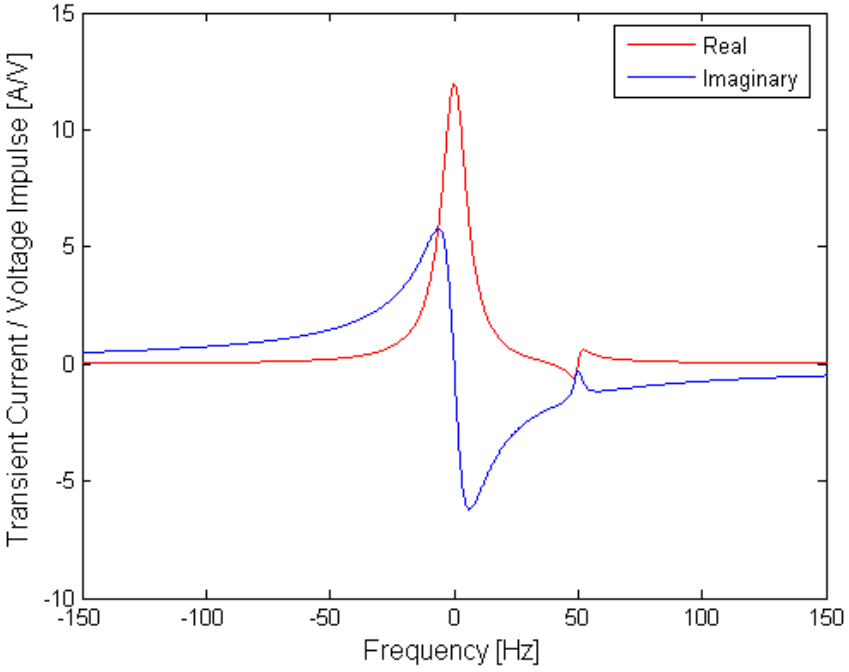

Figure 12: Calculated Admittance

The results of the admittance computed by FEA, without core losses included, are given in Figure 13 (Repo, 2007).

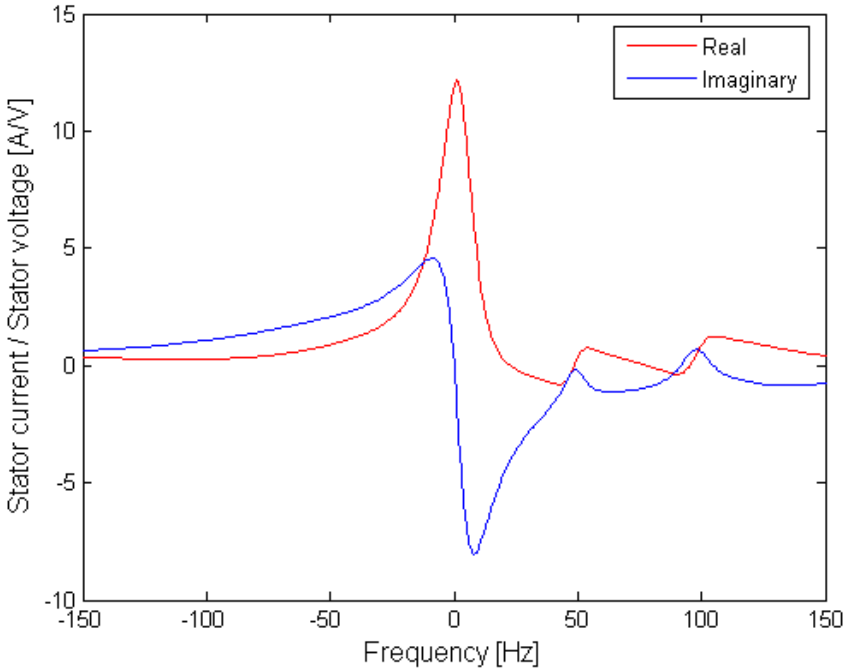

Figure 13: Admittance from FE Model

It is immediately obvious that the admittance from the FE results is more "squeezed", meaning the current-to-voltage ratio at higher frequencies is lower. It is suspected that since the skin effect in the rotor bars was not taken into account in the above model, the current calculated is higher than the "measured" FE current at higher frequencies. In addition, the knees of the curve around 100 Hz represent saturation, which has been ignored in the circuit model.

When the above figures are considered to represent measured values, the parameters for the equivalent circuit need to be estimated and are done so using the DE algorithm outlined earlier.

In the earlier stages of the thesis, the convergence was only possible if the stator and rotor leakage inductances were tied together. This is necessary as multiple solutions are possible if only the impulse test is considered. The last test run for the unconstrained case produced the following solution vector.

Table 3: Machine Parameters with Unconstrained $L_{\sigma r}$

Parameter	Original Model	Estimated Value
R_r (Ω)	6.5640E-02	6.6054E-02
$L_{\sigma s}$ (H)	7.4898E-04	6.9431E-04
L_m (H)	2.6302E-02	2.6372E-02
$L_{\sigma r}$ (H)	1.4671E-03	1.5283E-03
Y at 380 V, 50 Hz, no-load (S)	1.4443E-003 -1.1763E-001i	1.4443E-003 -1.1763E-001i

The parameters used for the algorithm are given in the following table.

Table 4: DE Parameters for Standard Small-Signal Model

Population Size	400	Upper Limits	10
Maximum Iterations	400	Lower Limits	1E-7
Crossover Constant	1	Target Cost	1E-8

Note that the solution converged to an error of 4.47E-6 once it reached the maximum number of iterations, from the cost function defined by

$$I = \sum_{i=1}^{N} \mathrm{Re}\{Y_{mi} - Y_{ci}\}^2 + \mathrm{Im}\{Y_{mi} - Y_{ci}\}^2 \tag{103}$$

where

Y_{ci} is the small-signal admittance calculated analytically for the ith point

Y_{mi} is the target small-signal admittance for the ith point

The parameters calculated were used to determine the admittance at no-load for the rated voltage and frequency. The calculated and target values of the admittance are identical and the solution converged. Yet there are significant errors in the leakage inductances. If the run is repeated, the algorithm converges to a difference set of inductance values. Similar results are reported by Repo (2008). Although the practise was adopted for the majority of this work, a workaround was discovered (as described in Section 4.5), results for which are provided in a later section. As a comparison to

Table 3, a test run with the constraint applied on the rotor inductance has been given below.

Table 5: Machine Parameters with Constrained $L_{\sigma r}$ Proportional to $L_{\sigma s}$

Parameter	Original Model	Estimated Value
R_r (Ω)	6.5640E-02	6.5640E-02
$L_{\sigma s}$ (H)	7.4898E-04	7.4898E-04
L_m (H)	2.6302E-02	2.6302E-02
Y at 380 V, 50 Hz, no-load (S)	1.4452E-003 -1.1771E-001i	1.4452E-003 -1.1771E-001i

The parameters used for the algorithm in both cases are given in the following table.

Table 6: DE Parameters for Standard Small-Signal Model

Population Size	400	Upper Limit	10
Crossover Constant	1	Lower Limit	1E-7
Maximum Iterations	400	Target Cost	1E-8
Actual Iterations	134	Actual Cost	8.97E-9
Execution Time (s)	98.1	Cost Evaluations	53600

The cost function used is defined as in (75) and (76). The first three rows of the above table show the parameters that were used to run the search algorithm (upper and lower limit refer to ranges of member variables). The bottom two rows show the number of iterations required, the cost obtained, time (in seconds) required for the algorithm to converge and the number of times the cost function was evaluated.

5.2 Core Loss Resistance Model with Fixed Steinmetz Coefficient

The core loss resistor was first defined as in (25), using the slip defined in (32). As opposed to Levi's model, the core loss in the rotor was included. However, it should be noted that as both rotor hysteresis and eddy current loss components are related to the slip, the losses in the rotor are very small near (and past) the rated operating point. With arbitrary k_{ce} and k_{ch} parameters, the calculated resistance, as a function of frequency is shown below.

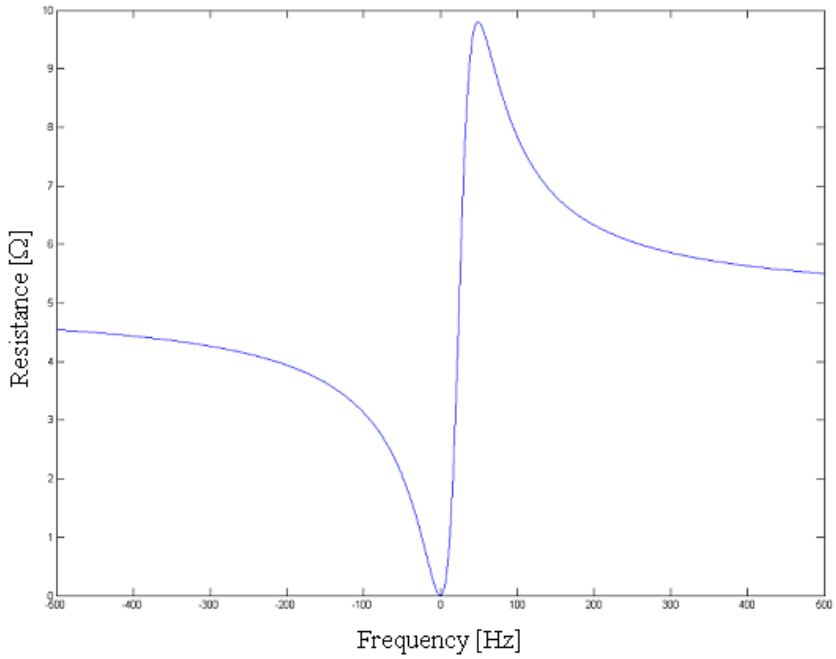

Figure 14: Core Loss Resistance vs. Frequency (Fixed Steinmetz Coefficient)

It is clear that the resistance is zero at DC and peaks at the supply frequency. As the frequency being considered increases, the "resistance" flattens out at a constant value. To better understand the effect of the hysteresis and eddy current loss coefficients, the sensitivity of the model was studied by setting the constants to values of 0.5 and 1.

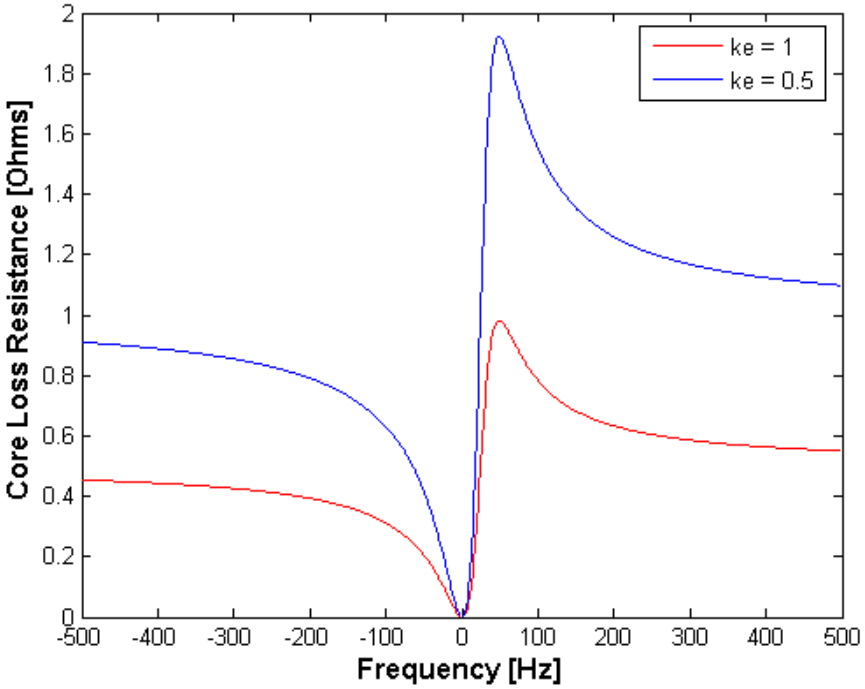

Figure 15: Sensitivity of Eddy Current Coefficient (Fixed Steinmetz Coefficient)

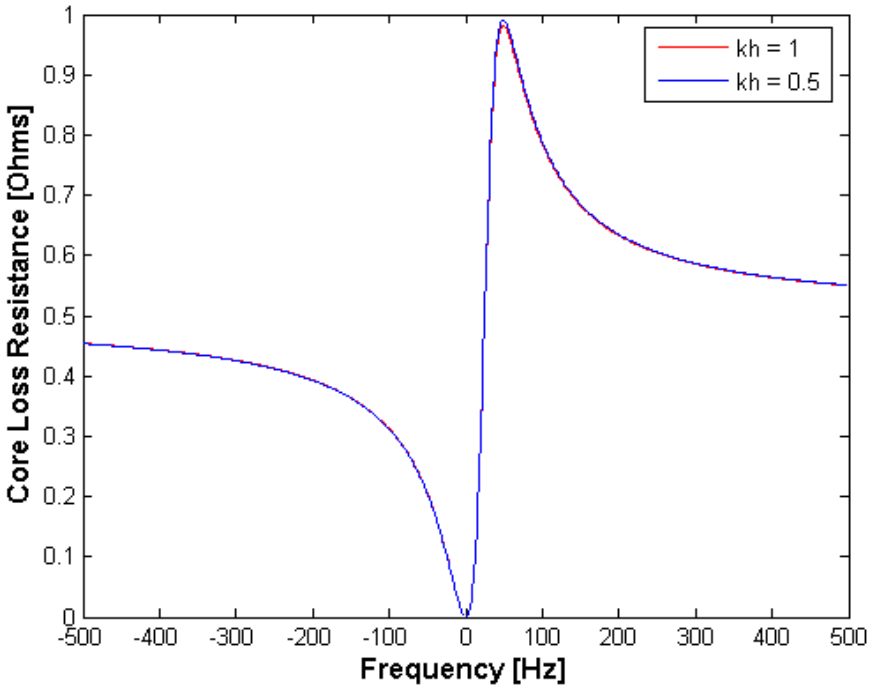

Figure 16: Sensitivity of Hysteresis Coefficient (Fixed Steinmetz Coefficient)

From the above, it can be seen that the core loss resistance (and therefore the power calculated), is much more sensitive to the eddy current coefficient. The result is not so surprising, considering the eddy current component dominates at higher frequencies. However, if the frequency is low enough (determined by the value of the coefficients), the hysteresis component will become more significant. Note that the lack of sensitivity to the hysteresis coefficient is exaggerated as it is typically two orders of magnitude larger than the eddy current loss coefficient.

5.3 Small-Signal Model Including Core Losses (Fixed Steinmetz Coefficient)

To study the range of the effect of the core loss resistance on the admittance, the core loss resistance was implemented in the small-signal model ((72) and (73)) and its coefficients varied from 10^{-7} to 10. The resulting admittances are plotted. In Figure 17, the darkest colors represent the high end of the coefficients and the lightest represent the low end.

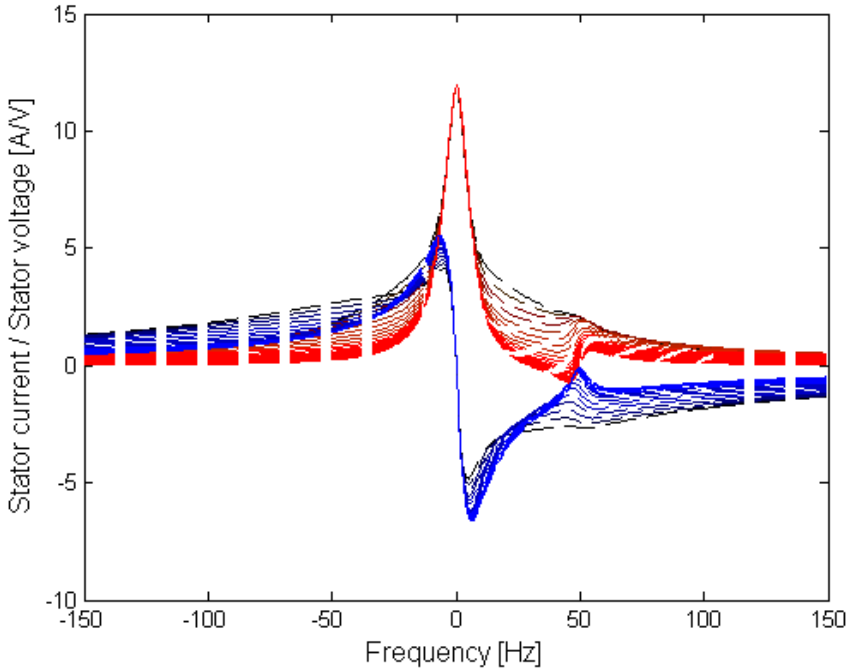

Figure 17: Range of Effect of Core Loss Resistance on Admittance

It was stated earlier that determining the core loss parameters from test data would either require the development of further tests or the measurement of another output from the machine. The statement will be justified here. As can be seen, the effect of the core loss resistor cannot easily be observed by the admittance of a voltage impulse. The same impulse voltage impulse was applied in all cases shown in the figure above. It can thus be concluded that the changes in current due to this type of signal will not be easily measurable and the stator current will be a poor indicator of core loss parameters. Nonetheless, the algorithm was tested with the two additional variables (k_{ce} and k_{ch}) and as predicted, it could not converge to the solution vector.

At this point, it was decided that more information is required to effectively calculate the core loss parameters. Studies were conducted using the FE models incorporating core losses into the magnetic field analysis, as developed and reported by Dlala (2008). The model determines the total iron losses in the machine. It also separates the core losses into stator and rotor components, as well as into the hysteresis, eddy current and excess loss components.

To study the effects of frequency on the core loss parameters, it was decided to conduct a series of tests with different frequencies and magnitudes of the supply. The machine was allowed to reach its steady state at no-load, at which point the core losses and the stator

current was determined. It should be noted that the flux in the machine was given an upper limit corresponding to the rated voltage and frequency. Appendix A provides the results of this study.

5.4 Parameters for Core Loss Small-Signal Model (Fixed Steinmetz Coefficient)

The approximate parameters of the standard model are first determined as per Section 4.2, using the cost function defined in (75) and (76). Note that the "measured" values of the admittance have the effects of core loss included[1]. The search algorithm then uses (produces) the following parameters (results).

Table 7: DE Parameters for Standard Small-Signal Model (Fixed Steinmetz Coefficient)

Population Size	300	Upper Limit	10
Crossover Constant	1	Lower Limit	1E-7
Maximum Iterations	300	Target Cost	1E-8
Actual Iterations	140	Actual Cost	2.17E-02
Execution Time (s)	75.1	Cost Evaluations	42000

Note that a slight modification to the search algorithm was made at this point. Previously, the algorithm terminated when either the maximum number of iterations ("failed") or the target cost was reached ("converged"). A third condition was added: terminate the algorithm if the standard deviation of the minimum costs of the lasts 50 iterations was less than 1E-5. In this case, the algorithm converges to values that may or may not have an acceptable cost (albeit it is greater than the target cost). What constitutes an appropriate cost is left to the user and must be based on engineering judgement. The modification will be utilised throughout the rest of the thesis.

With the obtained approximations for the standard machine parameters (shown in Table 10), the approximate core loss parameters are calculated using the cost function defined in (78) and (79). The search algorithm uses (produces) the following parameters (results).

Table 8: DE Parameters for Core Loss Steady-State Model (Fixed Steinmetz Coefficient)

Population Size	200	Upper Limit	10
Crossover Constant	1	Lower Limit	1E-7

[1] All "measured" admittance values in this section were computed using the **fixed** Steinmetz core loss model. This was done to allow a good convergence of small-signal model parameters, while being able to judge the accuracy of the model in determining core losses using the steady-state circuit. The parameters used are provided in Table 10.

Maximum Iterations	200	Target Cost	1E-8
Actual Iterations	80	Actual Cost	1.65E-01
Execution Time (s)	13.9	Cost Evaluations	16000

Finally, using these initial approximations, the core loss small-signal model and the cost function defined in (80), the five parameters are refined. The search algorithm uses (produces) the following parameters (results).

Table 9: DE Parameters for Core Loss Steady-State and Small-Signal Model (Fixed Steinmetz Coefficient)

Population Size	500	Upper Limit	$\{\theta'_m, \theta'_k\}\times 10^2$
Crossover Constant	1	Lower Limit	$\{\theta'_m, \theta'_k\}\times 10^{-2}$
Maximum Iterations	500	Target Cost	1E-8
Actual Iterations	213	Actual Cost	1.64E-01
Execution Time (s)	736	Cost Evaluations	106500

The approximate and calculated parameters obtained for the algorithm outlined in Section 4.2 are given in the table below.

Table 10: Machine Parameters with Core Losses (Fixed Steinmetz Coefficient)

Parameter	Original Model	Approx. Value	Estimated Value
R_r (Ω)	6.5640E-02	1.5423E-01	6.5813E-02
$L_{\sigma s}$ (H)	7.4898E-04	7.0427E-04	7.4729E-04
L_m (H)	2.6302E-02	6.3494E-02	2.6234E-02
k_{ch}	4.2394E-01	4.0948E-01	4.2405E-01
k_{ce}	1.5445E-03	1.5524E-03	1.5440E-03

The parameters calculated above produce the admittance curves shown in the following figure.

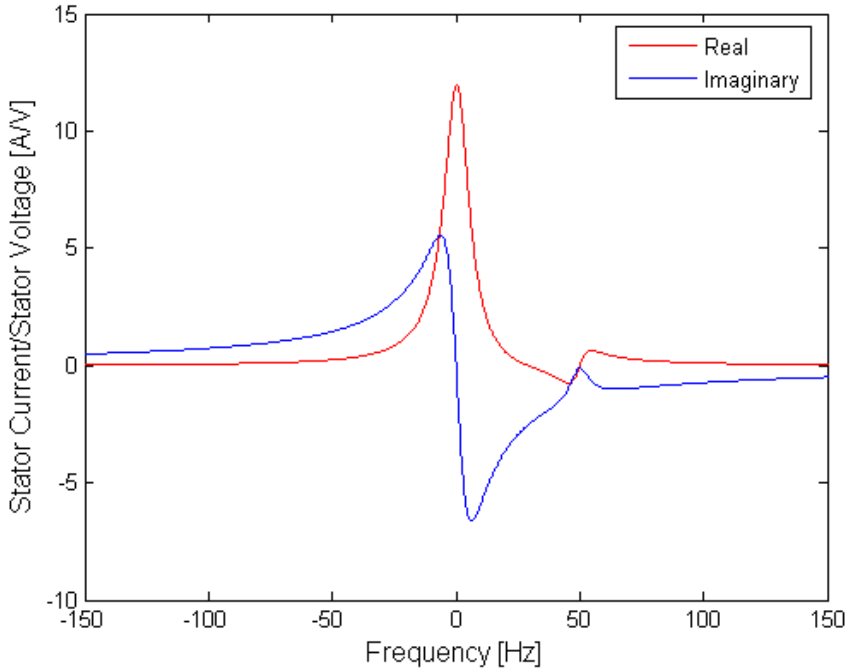

Figure 18: Admittance from Small-Signal Model with Core Losses (Fixed Steinmetz Coefficient)

The current response to the voltage in Figure 10, due to the above admittance, is shown in the following figure.

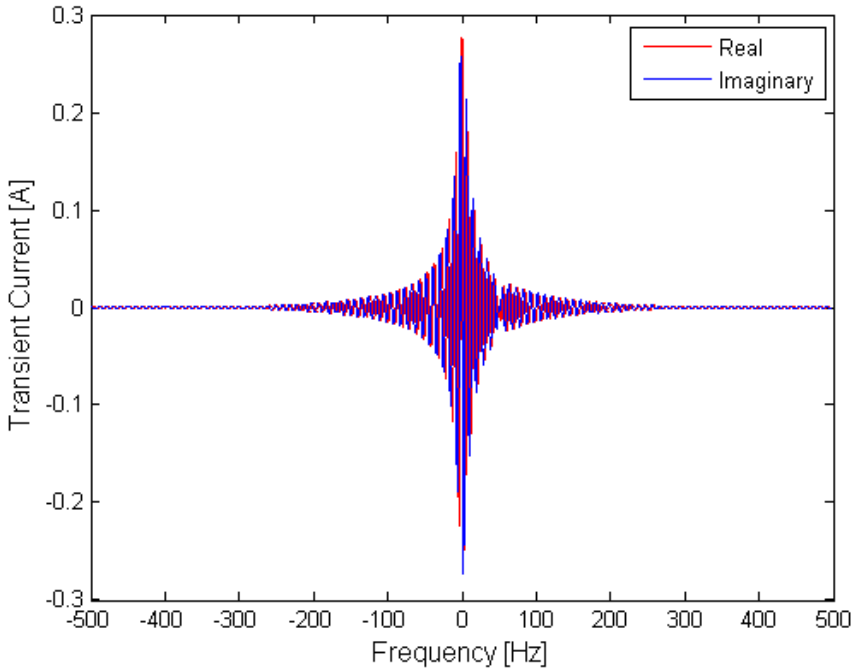

Figure 19: Current Response from Small-Signal Model with Core Losses (Fixed Steinmetz Coefficient)

As noted earlier, Repo and Dlala's works were recently combined to allow the admittance curves to be determined from an impulse voltage test using an FE model which

incorporated hysteretic material models, thereby including core losses. The admittance is given in the following figure.

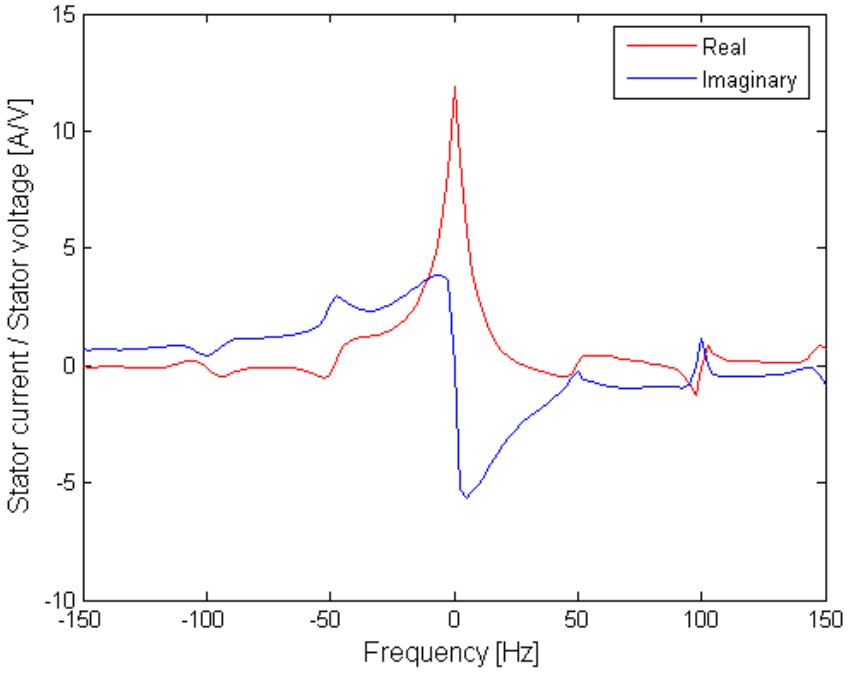

Figure 20: Admittance from FE Model with Hysteretic Materials

Although Figure 18 and Table 10 suggest the model performs well, a comparison of the core losses determined by the FE and analytical models shows a disparity. The losses calculated at different frequency and voltage points by both models are shown in the following figure.

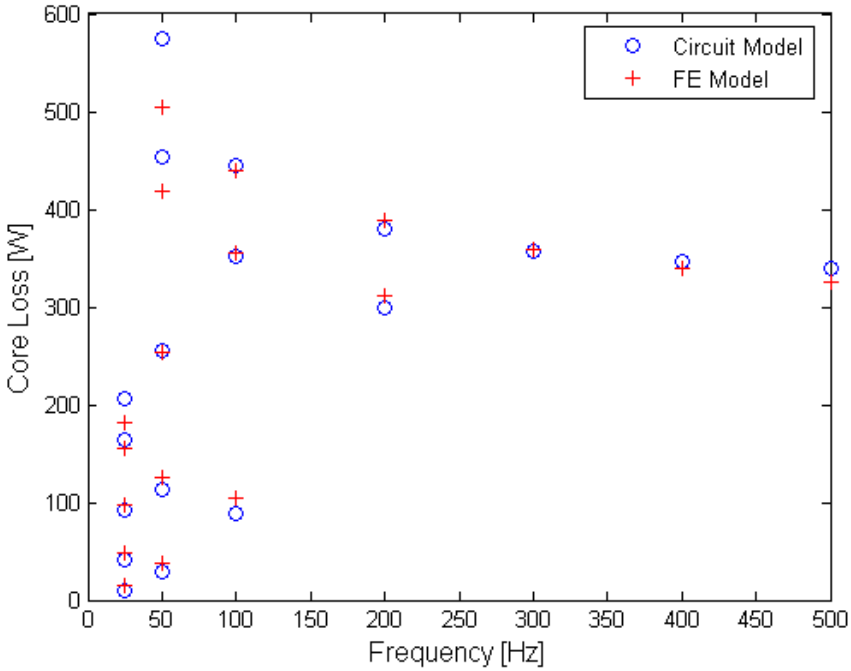

Figure 21: Core Losses Calculated by FE Model and Circuit Model (Fixed Steinmetz Coefficient)

Although the model converges and provides reasonable core losses in most cases, it is clear that at certain points, especially near the low frequency end, the calculation can be improved. Interestingly enough, the losses calculated from the circuit seem to be the worst at the rated frequency (especially at the higher voltages).

5.5 Core Loss Resistance Model with Variable Steinmetz Coefficient

The model can be improved by leaving the Steinmetz coefficient as a parameter to be determined. The model for the core loss resistance is derived in Section 4.3. Using the core loss resistance given in (85), the slip defined by (32), the core loss parameters given in Table 10 and a Steinmetz coefficient of 1.5, the calculated core loss resistance is shown in the following figure.

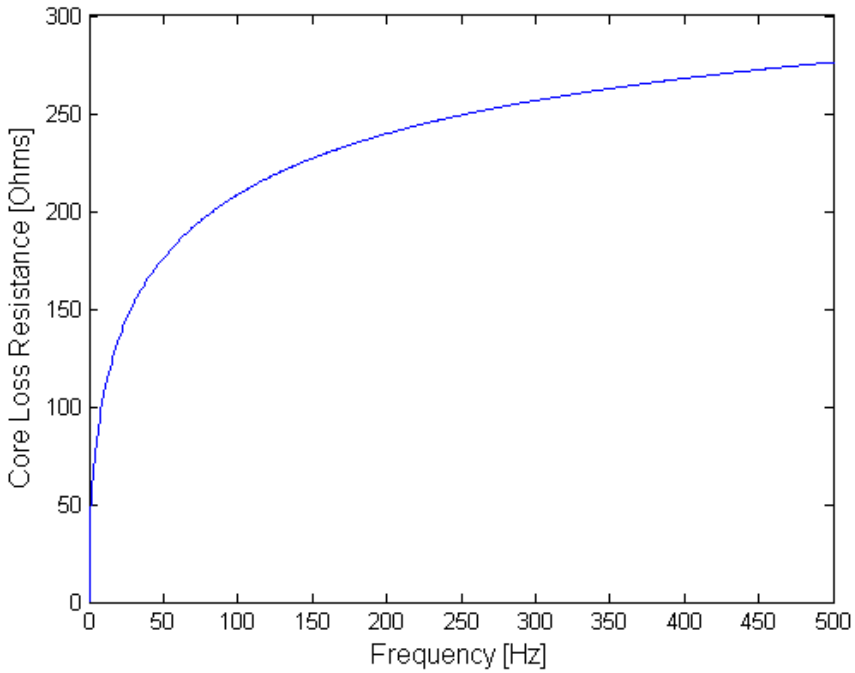

Figure 22: Core Loss Resistance with Variable Steinmetz Coefficient

Note that the shape of the curve is drastically different (and more reasonable) than that calculated for arbitrary constants equal, as in Figure 14 to Figure 16. For a constant slip (nearly zero, as in the case of a sinusoidal supply at no-load steady-steady conditions), the sensitivity of the core loss resistance was determined by setting the Steinmetz coefficient (m+1) to 1.5 and 2. The results are given in the following figure.

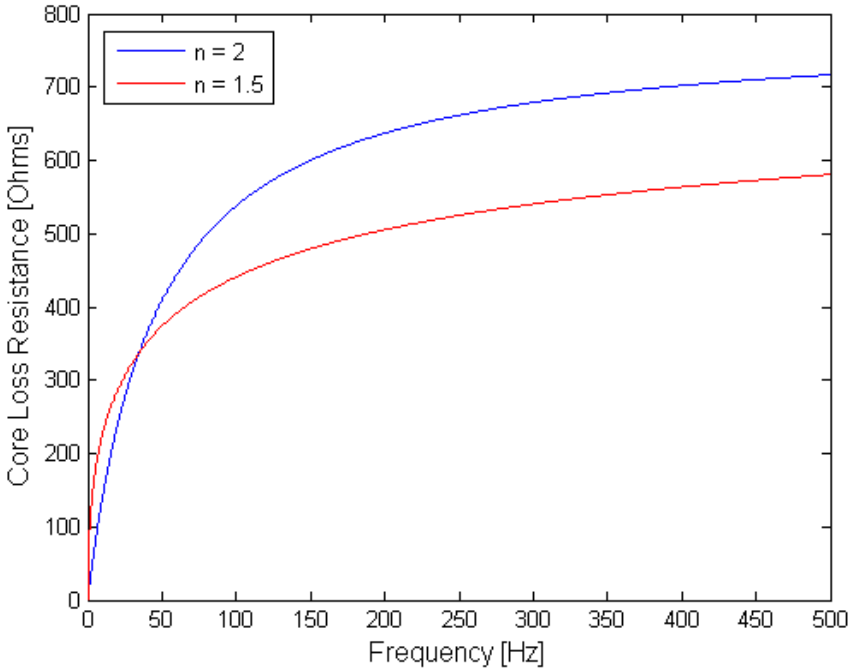

Figure 23: Sensitivity of Core Loss Resistance to Steinmetz Coefficient

5.6 Parameters for Core Loss Small-Signal Model (Variable Steinmetz Coefficient)

The admittance was determined using the small-signal model for a core loss resistance with a variable Steinmetz coefficient as described in Section 4.4. The results for the approximate standard machine parameters are first calculated. Note that the "measured" values of the admittance have the effects of core loss, with variable *n*, included[2]. The parameters (results) used (produced) by the DE algorithm are shown in the following table.

Table 11: DE Parameters for Standard Small-Signal Model (Variable Steinmetz Coefficient)

Population Size	300	Upper Limit	10
Crossover Constant	1	Lower Limit	1E-7
Maximum Iterations	300	Target Cost	1E-8
Actual Iterations	136	Actual Cost	1.51E-02
Execution Time (s)	71.4	Cost Evaluations	40800

The approximate core loss parameters are then determined using the cost function given in (78) and (79). The resulting approximations are given in Table 14. The search algorithm uses (produces) the following parameters (results).

[2] All "measured" admittance values in this section were computed using the **variable** Steinmetz core loss model. This model represents the final version of the core loss model used in the thesis. The parameters used are provided in Table 14.

Table 12: DE Parameters for Core Loss Steady-State Model (Variable Steinmetz Coefficient)

Population Size	300	Upper Limit $\{\theta_k, n\}$	{10, 10, 6}
Crossover Constant	1	Lower Limit $\{\theta_k, n\}$	{1E-7, 1E-7, 1}
Maximum Iterations	128	Target Cost	1E-8
Actual Iterations	300	Actual Cost	2.41E-02
Execution Time (s)	72.1	Cost Evaluations	38400

Using these initial approximations and the cost function defined in (80), the refined machine parameters are determined. The search algorithm uses (produces) the following parameters (results).

Table 13: DE Parameters for Core Loss Steady-State and Small-Signal Model (Variable Steinmetz Coefficient)

Population Size	600	Upper Limit $\{\theta_m, \theta_k, n\}$	$\{\{\theta'_m, \theta'_k\}\times 10^2, n'\times 10\}$
Crossover Constant	1	Lower Limit $\{\theta_m, \theta_k, n\}$	$\{\{\theta'_m, \theta'_k\}\times 10^{-2}, n'\times 10^{-1}\}$
Maximum Iterations	500	Target Cost	1E-8
Actual Iterations	322	Actual Cost	2.24E-02
Total Time (s)	1256	Cost Evaluations	193200

The approximate and calculated parameters obtained for the algorithm, as outlined in Section 4.4, are given in the table below.

Table 14: Machine Parameters with Core Losses (Variable Steinmetz Coefficient)

Parameter	Original Model	Approx. Value	Estimated Value
R_r (Ω)	6.5640E-02	1.5402E-01	6.6036E-02
$L_{\sigma s}$ (H)	7.4898E-04	7.0435E-04	7.5132E-04
L_m (H)	2.6302E-02	6.3451E-02	2.3895E-02
k_{ch}	3.6617E-01	3.5503E-01	3.6808E-01
k_{ce}	1.2787E-03	1.2910E-03	1.2769E-03
n	5.3076E-01	5.2909E-01	5.3220E-01

The parameters calculated above produce the admittance curves shown in the following figure.

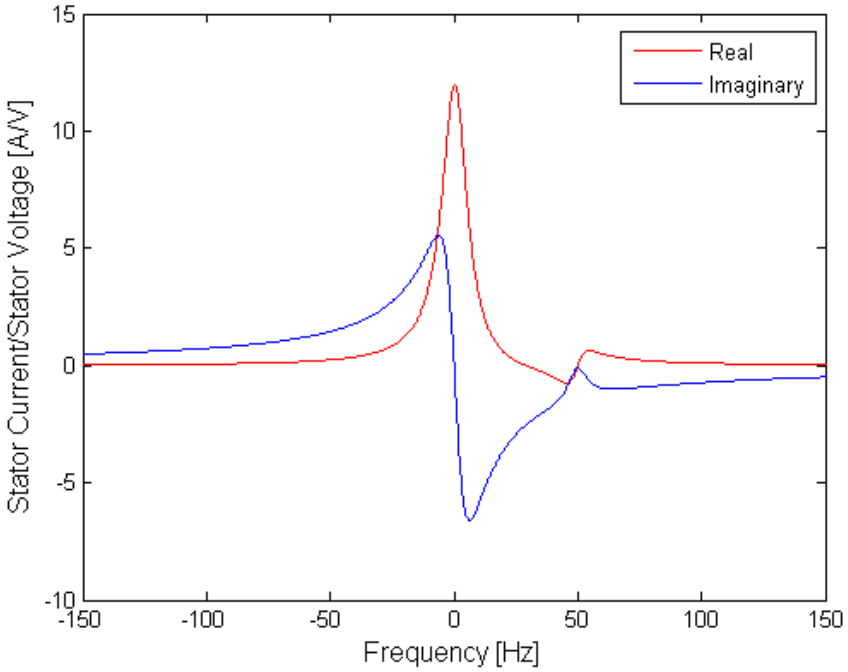

Figure 24: Admittance from Small-Signal Model with Core Losses (Variable Steinmetz Coefficient)

The current response to the voltage in Figure 10, due to the above admittance, is shown in the following figure.

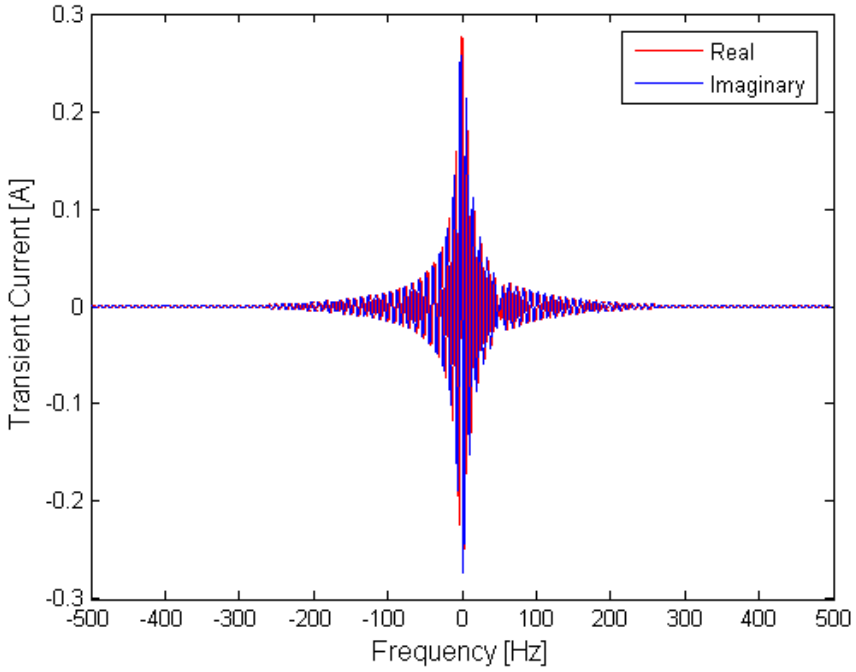

Figure 25: Current Response from Small-Signal Model with Core Losses (Variable Steinmetz Coefficient)

Finally, a comparison of core losses calculated by the analytical and FE models is shown in the following figure.

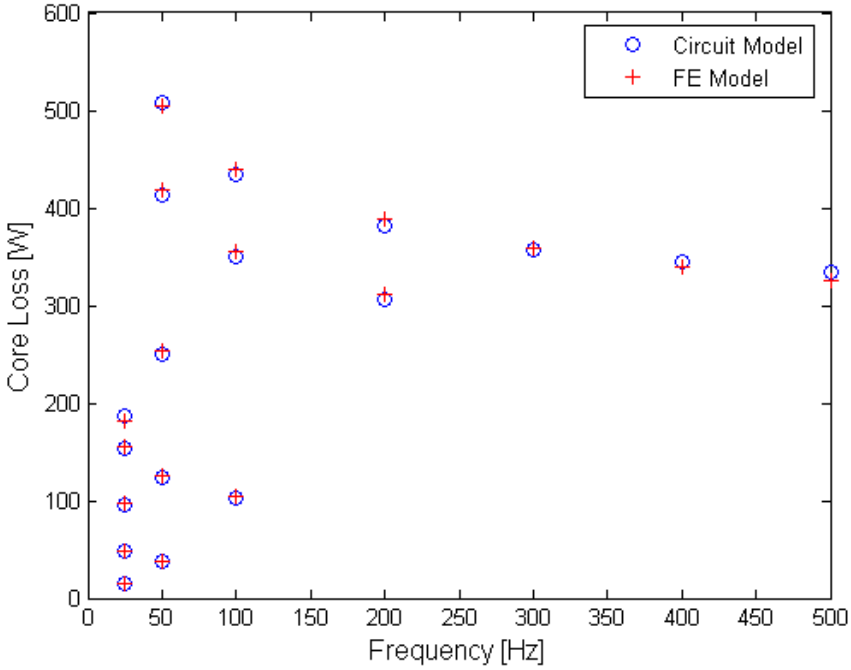

Figure 26: Core Losses Calculated by Circuit Model and FE Model (Variable Steinmetz Coefficient)

As can be seen from the figure above, the variable Steinmetz model produces an extremely good fit to the core losses given by the FE model. However, the total solution times (for both fixed and variable *n*) are rather long. Furthermore, in all cases, the stator and rotor leakage reactances have been related.

5.7 DC Step Voltage Test and the Combined Method

A method for obtaining the standard circuit parameters based on DC step voltage test was outlined in Section 3.9. Although the method is an iterative one, it is more direct and therefore faster than the DE method used with the small-signal model. As outlined in Section 4.5, a Combined Method, using results from the DC step voltage test and the impulse response test can be used to determine stator and rotor leakage inductances independently.

To obtain the "measured" values used in the method, a SimuLink Model of the induction machine at standstill was employed. The model was built based on the circuit of Figure 9 and is shown in the figure below.

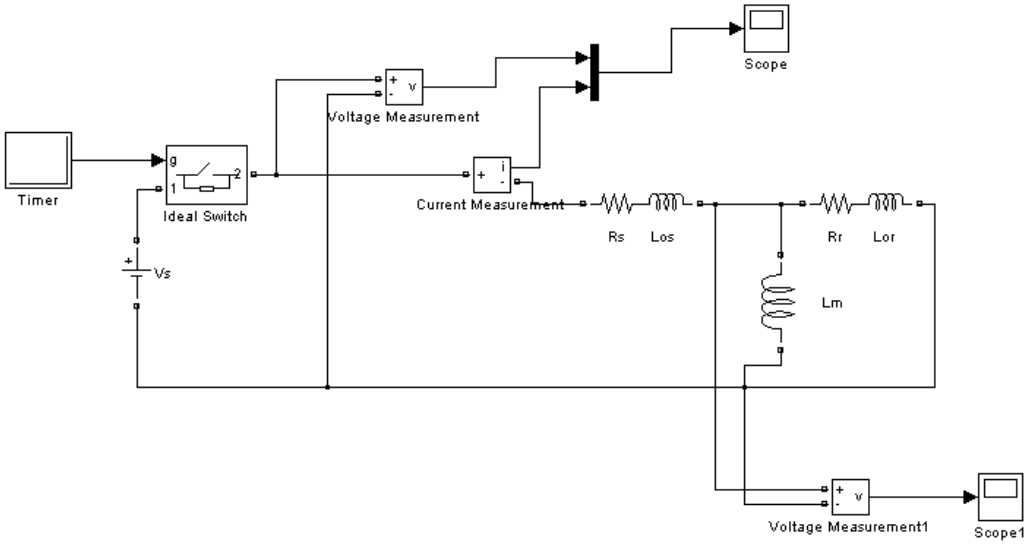

Figure 27: Induction Machine Model with DC Step Voltage Source

It is to be noted that this model does not take core loss resistance into account. However, the effect of this resistance is negligible; the model serves to give a good approximation of the stator current in response to a step voltage. The parameters determined will certainly be good approximations for the standard machine parameters.

The applied voltage was set to 1% of the rated. The machine parameters used are given in Table 2. Both the applied step voltage and its current response are given in the figure below.

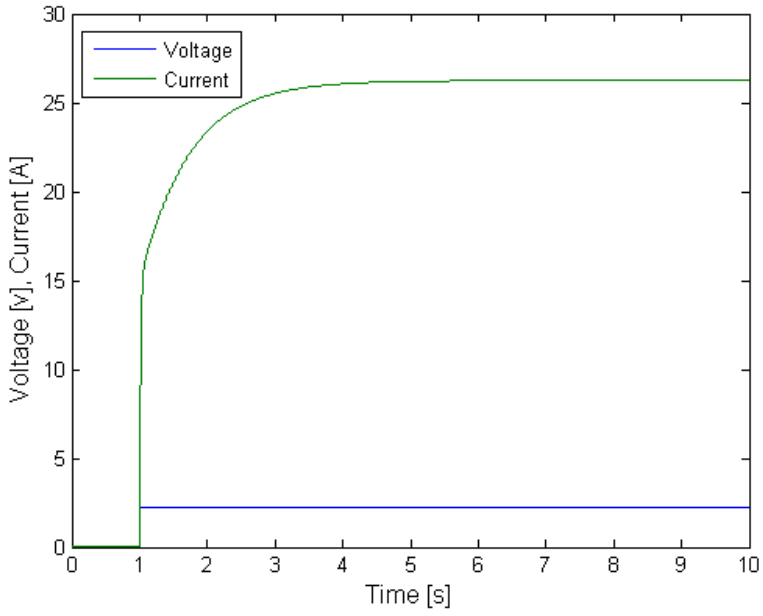

Figure 28: DC Step Voltage Test for Induction Machine

The following four sample points were used.

Table 15: Sample Points for DC Step Voltage Test

t (s)	I_s (A)
0.050	15.18
0.100	16.37
0.150	17.04
0.200	17.65

The results of the method outlined in Section 3.9 are given below.

Table 16: Machine Parameters from DC Step Voltage Test $L_{\sigma r}$ Proportional to $L_{\sigma s}$

Parameter	Original Model	Estimated Value
R_s (Ω)	8.3570E-02	8.3582E-02
$L_{\sigma s}$ (H)	7.4898E-04	7.4871E-04
L_m (H)	2.6302E-02	2.6304E-02
R_r (Ω)	6.5640E-02	6.5642E-02
$L_{\sigma r}$ (H)	1.4671E-03	1.4668E-04

In addition, the initial results required for the method outlined in Section 4.5 are given below. Note that both these methods required the same amount of time (0.016s) and iterations (41) to converge. The error tolerance was set to 1E-7.

Table 17: Machine Parameters from DC Step Voltage Test

Parameter	Original Model	Estimated Value
R_s (Ω)	8.3570E-02	8.3580E-02
L_s (H)	2.7051E-02	2.7051E-02
T_s (H/Ω)	3.2369E-01	3.2365E-01
T_r (H/Ω)	4.2305E-01	4.2305E-01
k	9.5966E-01	9.5967E-01

At this point, the DE algorithm was used to find an acceptable value for R_r. The relationships determined by the step voltage test were used to determine approximations, based on R_r, for the remaining standard parameters. The parameters and results for the DE algorithm are given in the following table.

Table 18: DE Parameters for Standard Small-Signal Model (Combined Method)

Population Size	50	Upper Limit	10
Crossover Constant	1	Lower Limit	1E-7
Maximum Iterations	300	Target Cost	1E-8
Actual Iterations	79	Actual Cost	29.3
Execution Time (s)	7.77	Cost Evaluations	3950

The approximate parameters are given in Table 21. Note that although a good convergence to the parameters was reached, the cost shown in the above table is quite high. This is because the effect of the core loss parameters has not yet been included. The approximate core loss resistance parameters are now determined. The following table provides the details for the DE algorithm.

Table 19: DE Parameters for Core Loss Steady-State Model (Combined Method)

Population Size	300	Upper Limit $\{k_{ch}, k_{ce}, n\}$	{10, 10, 6}
Crossover Constant	1	Lower Limit $\{k_{ch}, k_{ce}, n\}$	{1E-7, 1E-7, 1}
Maximum Iterations	200	Target Cost	1E-8
Actual Iterations	126	Actual Cost	2.26E-02
Execution Time (s)	70.4	Cost Evaluations	37800

Finally, the approximate core loss parameters, along with the relationships given by the step voltage test, were used to solve the parameters for the small-signal model with core losses included, using a variable Steinmetz coefficient. Note that in this case, the search reduced to a five parameter search (stator resistance is known and magnetising inductance can be calculated). The following DE parameters were used.

Table 20: DE Parameters for Core Loss Steady-State and Small-Signal Model (Combined Method)

Population Size	500	Upper Limit $\{\boldsymbol{\theta}_m, \boldsymbol{\theta}_k, n\}$	$\{\{\boldsymbol{\theta}'_m, \boldsymbol{\theta}'_k\}\times 10^{2}, n'\times 10\}$
Crossover Constant	1	Lower Limit $\{\boldsymbol{\theta}_m, \boldsymbol{\theta}_k, n\}$	$\{\{\boldsymbol{\theta}'_m, \boldsymbol{\theta}'_k\}\times 10^{-2}, n'\times 10^{-1}\}$
Maximum Iterations	500	Target Cost	1E-8
Actual Iterations	207	Actual Cost	2.26E-02
Execution Time (s)	864	Cost Evaluations	103500

The following machine and core loss parameters (and their approximations) are thus obtained.

Table 21: Machine Parameters with Combined Method

Parameter	Original Model	Approx. Value	Estimated Value
R_s (Ω)	8.3570E-02	8.3580E-02	8.3580E-02
$L_{\sigma s}$ (H)	7.4898E-04	7.4898E-04	7.1376E-04
R_r (Ω)	6.5640E-02	6.5717E-02	6.5638E-02
$L_{\sigma r}$ (H)	1.4671E-03	1.4671E-03	1.5000E-03
L_m (H)	2.6302E-02	2.6302E-02	2.6268E-02
k_{ch}	3.6617E-01	3.6620E-01	3.6626E-01
k_{ce}	1.2787E-03	1.2785E-03	1.2787E-03
n	5.3076E-01	5.3081E-01	5.3085E-01

The parameters calculated above produce the admittance curves shown in the following figure.

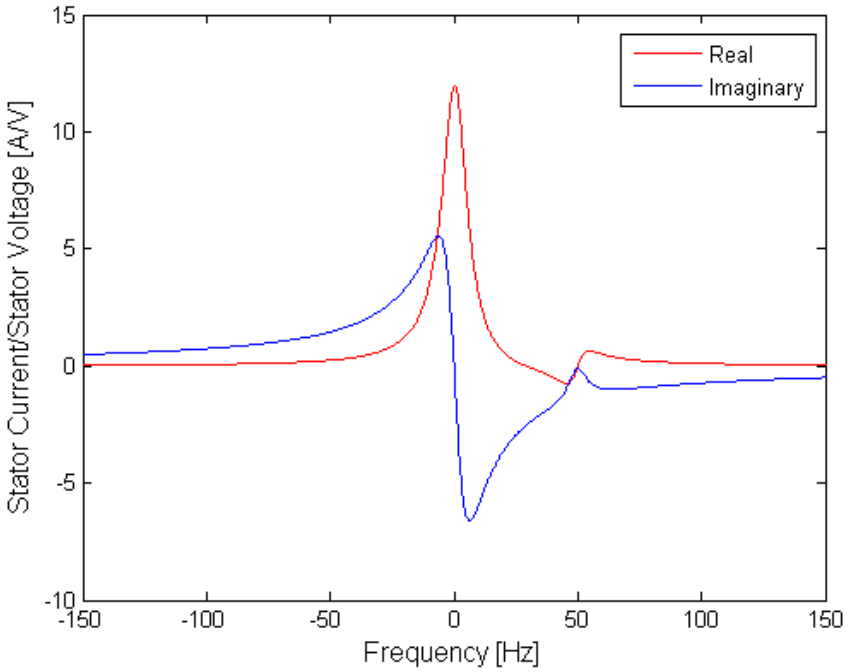

Figure 29: Admittance from Small-Signal Model with Core Losses (Combined Method)

The current response to the voltage in Figure 10, due to the above admittance, is shown in the following figure.

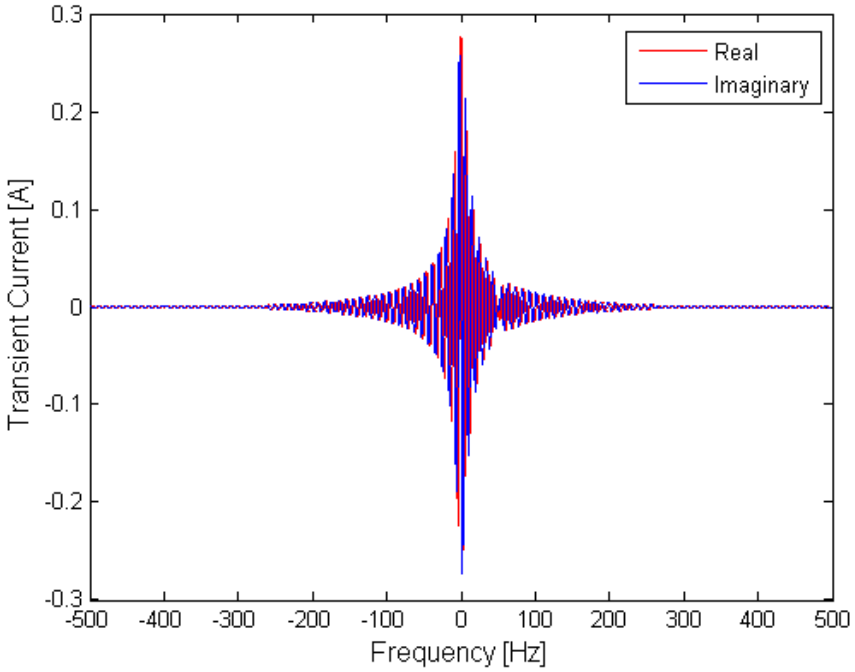

Figure 30: Current Response from Small-Signal Model with Core Losses (Combined Method)

A comparison of core losses calculated by the analytical and FE models is shown in the following figure.

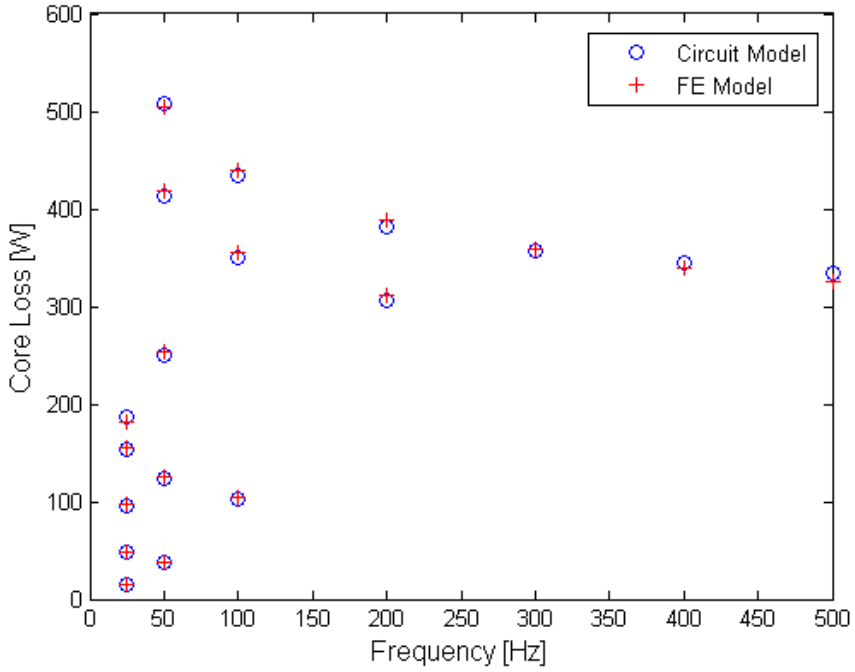

Figure 31: Core Losses Calculated by Circuit Model and FE Model (Combined Method)

5.8 Summary of Algorithm Results

This section, along with sections 5.4, 5.6 and 5.7 provide results of three different algorithms presented and compared during the thesis. These results are now summarised.

Each algorithm presented contained three different components, or sets, of searches. To compare the algorithms, the sum of all DE iterations required was obtained. Furthermore, the total number of cost function evaluations for each algorithm was obtained. It is worth noting that although each component has different computational requirements (different cost functions and parameters), a comparison is still possible given that all three algorithms used similar DE parameters for each component. To put the iterations in perspective, the total time required to run the algorithm as also determined. The results are given in the following table.

Table 22: Tabulated Results of Presented Algorithms

Algorithm	Cost Evaluations	Iterations	Execution Time (s)	Minimum Error
Fixed Steinmetz Coefficient	164500	433	825	1.65E-01
Variable Steinmetz Coefficient	272400	586	1400	2.24E-02
Combined Method	145250	412	942.234	2.26E-02

5.9 Rated Operating Point Test

A test was done to compare the outputs of the FE model near the rated operation point with that of the final core loss models described in this thesis.
The results are shown in the table below.

Table 23: Rated Operating Point Test

Model Type	FE (rated load)	Analytical (rated load)	FE (no load)	Analytical (no load)
Line Voltage (V)	380	380	380	380
Line Current (A)	71.26	70.60	23.01	25.82
Core Loss (W)	624.79	372.51	417.58	377.49
Torque (Nm)	244.27	242.13	N/A	N/A
Frequency (Hz)	50	50	50	50
Slip	0.02	0.02	0	1e-8

Note that, as outlined in Section 1.2, the core loss calculation in the FE model includes the core and stray load loss. Therefore, the losses calculated by the analytical model are appropriately smaller for the loaded case. Without the inclusion of the stray load loss resistors, the calculated losses decrease. As more current is drawn by the machine, the air-gap voltage is reduced and the power loss across the core loss resistance is lowered.

Chapter 6
Conclusion

6.1 Summary

The key points of the thesis will now be summarised. The thesis utilised numerous tools and concepts found throughout the literature and made available by the Electromechanics Research Group.

The DE search algorithm has been widely publicised and is available online. It was used heavily to determine parameters of the multivariate searches. In most cases, it was found that good convergence characteristics could be maintained by using roughly 100 population members per variable to be optimised. The iterations were usually limited to the same number as the population size, and the crossover constant was usually set to 1.

The standard induction machine circuit models were used to determine approximate values of the machine parameters. At first, these standard parameters were determined by using the small-signal model with an applied voltage impulse and the DE algorithm. However, it was determined that a DC step voltage test would provide significantly better results in less time and fewer calculations. It was therefore decided to abandon the small-signal model for this purpose.

A model for the core loss resistance was determined from the literature, based on a core power loss model with a fixed Steinmetz coefficient. A small-signal model, including this core loss resistance, was then developed from the dynamic circuit. However, the small-signal model was of limited use on its own to determine these parameters. Therefore, the parameters of this resistance were determined by comparing its power loss in the steady-state circuit with the core losses measured by the FEA.

To do so, however, it was necessary to develop an iteration sequence where the approximate circuit parameters were first determined. These allowed the approximate core loss resistance parameters to be calculated. Finally, the core loss and the standard model parameters were refined collectively using the developed small-signal model and core power loss measurements. The small-signal model was inherently verified as it provided a reasonable fit to the admittance determined from the FEA, given allowances for the lack of saturation and skin effect. However, the core losses determined by the model gave poor performance at the low frequency end, where the hysteresis losses dominate.

It was therefore decided to develop a model for the core loss resistance with a variable Steinmetz coefficient, which required the air-gap voltage to be known. The implementation of this model required another layer of iterations to be implemented, whereby the initial guess of the air-gap voltage was determined by the standard steady-state circuit model and later refined with the core loss model.

The overall algorithm then produces reasonable parameters for the circuit models with core losses included. The analytical models and parameters have been verified by the core losses calculated by the FEA, as well as by a rated operation point test.

The DC step voltage test was initially used to reduce the computation time of the algorithm. However, the relationships determined by this test also allowed the stator and rotor leakage inductances to be determined independently. All eight parameters for the machine can now be determined without any prior knowledge regarding their values.

The final algorithm is outlined:

- Run the DC step voltage test and obtain values for the stator resistance, the stator inductance, the stator and rotor time constants and the coupling coefficient.

- Run the DE search to determine an approximate value for the rotor resistance.

- Use the rotor time constant and the coupling coefficient to determine approximate values for the magnetising inductance and the rotor leakage inductance.

- Run the DE search to determine approximate values for the hysteresis and eddy current loss coefficients and the Steinmetz coefficient.

- Run the DE search to determine the refined parameters for the rotor resistance, stator leakage inductance, the hysteresis and eddy current loss coefficients and the Steinmetz coefficient.

- Determine the magnetising inductance and the rotor leakage inductance from the rotor time constant and coupling coefficient. The stator resistance is assumed to be known from the DC step voltage test.

6.2 Accuracy of the Models

Two different core loss models and three different algorithms to determine the circuit parameters for an induction machine have been presented in this thesis.

The first algorithm, based on the impulse voltage test, uses the core loss resistance model with a fixed Steinmetz coefficient. The parameters obtained from this algorithm are shown in Table 10 and show reasonable values. The admittance curves, current response and core losses are shown in Figure 18, Figure 19 and Figure 21. The admittance curves obtained from FEA are shown in Figure 20. It is apparent from the figures that although the calculated losses show a good fit to the values obtained from FEA, there is significant disagreement in the lower frequency range. The range includes the standard operating frequency. The final error for this model was shown to be 0.165, or 16.5%. Clearly, it was necessary to upgrade the model.

The second algorithm, also based on the impulse voltage test, uses the core loss resistance model with a variable Steinmetz coefficient. The parameters obtained from the algorithm are shown in Table 14 and also show reasonable values. The admittance curves, current response and core losses are shown in Figure 24, Figure 25 and Figure 26. The resistance model shows a significant improvement in the calculation of the core losses. The final error obtained for this model was 0.0224 or 2.24%.

Finally, a third algorithm is provided that combines the step and impulse voltage tests to determine machine parameters. The core loss resistance models are similar to the second algorithm. The admittance curves, current response and core losses are shown in Figure 29, Figure 30 and Figure 31. Although the results are similar, a significant improvement is observed in algorithm behaviour and is discussed in the next section. The final error obtained is 2.26%.

Based on the results provided in the tables of Chapter 5, it is clear that the core losses from the models provided in this thesis match the core losses determined by FE models with a reasonable degree of accuracy. Note that although the admittance curves allowed convergence to reasonable circuit parameters, these "measured" curves were actually determined by the same analytical models for which parameters were being determined.

To allow the admittance curves obtained from the FE models to be used as the target curves, skin effect and saturation must be included in the analytical models.

6.3 Algorithm Characteristics

The first algorithm requires 433 DE iterations and 164,500 evaluations of the cost function. In addition, it required 825 seconds to determine the machine parameters, albeit with significant error. The second algorithm requires 586 iterations and 272,400 evaluations of the cost function. The total time required to run the algorithm was 1400 seconds. However, the errors are significantly reduced. Finally, the third algorithm required 412 DE iterations. It contained 41 initial (and fast) iterations to converge to results from the step voltage test. These results required 0.016 seconds to evaluate. The DE cost function was evaluated 145,250 times and the total execution time was 942 seconds. Note that the second and third algorithms contained an additional iteration to simultaneously determine the air-gap voltage and core loss resistance; although 3 to 8 iterations were required 80% of the time, an instance of 25 iterations was also recorded.

The first algorithm was the fastest in determining the machine parameters. However, it also produced the greatest amount of error. The second algorithm reduced the error, but nearly doubled the computation time. The third algorithm maintains the increased accuracy, but only showed a 14% increase in computation time from the first algorithm. This algorithm (with the associated core loss model) is therefore recommended.

6.4 Self-Evaluation

The aim of this thesis was to include iron losses and their dependency on supply frequency in analytical models for an induction machine. These models are eventually to be used in converters meant to minimise the total loss in an electric drive. It was decided to focus primarily on core loss, as opposed to stray load loss, as the latter involves phenomena present in the copper as well as the iron.

On the whole, the models and algorithms provide good results to the measured values for the no-load case. Therefore, the objective of gaining understanding of the frequency dependency of the core losses has been fulfilled. In addition, the outlined algorithms converge within a reasonable timeframe and are adept at providing accurate parameters. There are, however, some shortcomings in the outlined models and procedures.

It is somewhat unfortunate that the effect of the core loss resistance was not very pronounced in the small-signal model. Although the core loss parameters could still be determined, doing so required the use of FEA. It is preferred that they eventually be determined from measurable stator values. Unfortunately, the impulse response test is not very fruitful in this regard. However, the small-signal and steady-state models, with the core losses, are still useful to refine the overall circuit parameters. To produce a significant effect in stator measurements, new models for different kinds of tests are required and are discussed in the following section.

6.5 Future Work

First, the stray load losses should be included in the dynamic and steady-state models for the machines. Various references [(Honsinger, 1980) & (Sousa et al., 1992)] suggest that these losses may be modeled in a much the same way as the core losses. Although initially disregarded, it is worth conducting a new FE study for the 37kW machine, where the losses at the rated load are determined for various frequency and voltage points. The stray-load loss parameters for the machine may then be determined based on the results.

Second, the saturation and skin effect must be modelled. The model does not then need to be considered linearised around the operating frequency. As such, new models can be generated to determine the behaviour of iron losses with non-sinusoidal supplies. Their dependencies on switching frequency can then be determined and circuit elements added to the models as appropriate.

Third, it is worth studying the possibility of incorporating iron losses in models used for step voltage tests. As the behaviour based on DC sources is quite well understood (the machines behave very similar to transformers), these tests may allow significant improvements in computation time.

Fourth, tests should be determined that highlight the effect of core losses on the possible output variables. These tests may be based on measurement of both stator current and output torque. Algorithmic schemes can then be developed (as they were throughout this thesis) to efficiently use this test data and allow the relevant parameters to be determined, without the use of FE data.

Finally, it is important to study the generality of these models by applying them to various types of machines. It is also necessary to obtain actual test data from the machine and apply the developed algorithms to determine parameters for the developed models.

With these five additions, relatively accurate models and processes can be developed to minimise the losses in induction machines driven by PWM supplies. With due experience, the models can then be expanded for other forms of control algorithms, where the fundamental and switching frequency of the supply may not be defined.

References

Alger, P.L. (1965a), "Discussion on Stray Load Losses in Squirrel-Cage Induction Motors", *Proceedings of the IEE*, vol. 112, pp. 1750-1759.

Alger, P.L. (1965b), "The Nature of Induction Machines", New York, N. Y.: Gordon and Breach, Science Publishers, Inc.

Alger, P.L., Angst, G. & Davies, E.J. (1957), "Stray Load Losses in Polyphase Induction Machines", *Transactions of the AIEE*, vol. 78, pp. 349-357.

Barnes, M.L. & Gross, C.A. (1995), "Comparison of Induction Machine Equivalent Circuit Models", *Proceedings of the 27th Southeastern Symposium on System Theory*, pp. 14-17, 12-14 March 1995.

Belloc, C., Zhang, H., Vagapov Y., Moreno, P. (2006), "A Step Voltage Response Method for Identification of Induction Motor Parameters at Stand Still", *IEEE International Conference on Electro/information Technology, May 2006*, pp. 109-111.

Bertotti, G. (1988), "General properties of power losses in soft ferromagnetic materials", *IEEE Trans. Magnetics*, vol. 24, no.1, pp. 621-630, January 1988.

Bird, B.M. & Holgate, A. (1967), "Discussion on Determination of Load Losses and Torques in Squirrel Cage Induction Motors", *Proceedings of the IEE*, vol. 114, pp. 1085-1088.

Bird, B.M. (1964), "Measurement of stray load losses in squirrel-cage induction motors", Proceedings of the IEE, vol. 111, no. 10, pp. 1697-1705.

Boglietti, A., Cavagino, A., Ferraris, L. & Lazzari, M. (2007), "Induction Motor Equivalent Circuit Including the Stray Load Losses in the Machine Power Balance", *Annual Conference of the IEEE Industrial Electronics Society*, pp. 1250-1255, 5-8 November 2007.

Boldea, I. & Nasar, S.A. (1987), "Unified treatment of core losses and saturation in the orthogonal-axis model of electrical machines," *IEE Proceedings, Pt. B*, vol. 134, no. 6, pp. 355-363.

Bonnet, A.H. (1980), "Understanding Efficiency in Squirrel-Cage Induction Motors", *Transactions of the IEEE*, vol. IA-16, pp. 476-483.

Bose, B.K. (1986), "Power Electronics and AC Drives", Englewood Cliffs, N. J.: Prentice-Hall. ISBN 0-13-686882-7.

Chalmers B. & Williamson A. (1991), "A.C. Machines: Electromagnetics and Design", Taunton, Somerset, England: Research Studies Press Ltd., ISBN 0-86380-115-3.

Chalmers, B.J. & Williamson, A.C. (1958), "The Measurement of Induction-Motor Stray Loss and its Effect on Performance", *Proceedings of the IEE*, vol. 1050, pp. 69-75.

Chalmers, B.J. & Williamson, A.C. (1963), "Stray Losses in Squirrel-Cage Induction Motors – Validity of Reverse-Rotation Test Method", *Proceedings of the IEE*, vol. 110, pp.1773-1777.

Chen, Y. & Pillay, P. (2002), "An improved formula for lamination core loss calculations in machines operating with high frequency and high flux density excitation", *IEEE 37th IAS Annual Meeting.* vol. 2, pp. 759-766, 13-18 October 2002.

Cochran, P.L. (1989), "Polyphase Induction Motors", New York, N.Y.: Marcel Dekker, Inc.

Couto, E.B. & Aguiar, M.L. (1998), "Parameter Identification of Induction Motors Using DC Step Excitation at Standstill", *IEEE International Symposium on Industrial Electronics*, vol. 2, pp. 468-471, 7-10 July 1998.

Dlala, E. (2008a), "A Simplified Iron Loss Model for Laminated Magnetic Cores", *IEEE Transactions on Magnetics*, vol. 44, no. 11.

Dlala, E. (2008b), "Magnetodynamic Vector Hysteresis Models For Steel Laminations of Rotating Electrical Machines", Doctoral Dissertation, Helsinki University of Technology, Department of Electrical Engineering, TKK-DISS-2448, ISBN 978-951-22-9277-6, [Available Online: http://lib.tkk.fi/Diss/2008/isbn9789512292776].

Hildebrand, N.E. & Roehrdanz H. (2001), "Losses in Three-Phase Induction Machines Fed by PWM Converter", *IEEE Transactions on Energy Conversion*, vol. 16, no. 3, pp. 228-233.

Hinkkanen, M. (2008), "Dynamic IM Model Taking Into Account Hysteresis Losses", Unpublished. Available at Power Electronics Laboratory, Helsinki University of Technology.

Honsinger, V.B. (1980), "Induction Motors Operating from Inverters", *Proceedings of the IEEE Industrial Applications Society Annual Meeting IAS*, pp. 1276-1285.

IEEE Power Engineering Society (2004), "IEEE Standard Test Procedure for Polyphase Induction Motors and Generators", IEEE Std 112-2004, New York, N.Y.: IEEE.

Jeon, S.L. (2007), "Non-sinusoidal power theory in a power system having transmission lines with frequency-dependent resistances", IET Gener. Trans. Distrib., vol. 1, no. 2, pp. 331-340.

Jimoh, A.A.,S, Findlay, R.D., SM & Poloujadoff, M. (1985a), "Stray Losses in Induction Machines: Part I, Definition, Origin and Measurement", *IEEE Transactions on Power Apparatus and Systems*, vol. PAS-104, no. 6, pp. 1500-1505, June 1985.

Jimoh, A.A.,S, Findlay, R.D., SM & Poloujadoff, M. (1985b), "Stray Losses in Induction Machines: Part II, Calculation and Reduction", *IEEE Transactions on Power Apparatus and Systems*, vol. PAS-104, no. 6, pp. 1506-1512, June 1985.

Jones, C.V. (1967), "The Unified Theory of Electrical Machines", London, U.K.: Butterworth & Co. (Publishers) Ltd.

Koch, C.J. (1932), "Measurement of Stray Load Loss in Polyphase Induction Motors", *Proceedings of the IEE*, vol. 51, pp. 756-763.

Kron, G. (1951), "Equivalent Circuits of Electrical Machinery", New York, N. Y.: John Wiley & Sons, Inc.

Lamine, A. & Levi, E. (2004), "Dynamic Induction Machine Modelling Considering the Stray Load Losses", *39th International Universities Power Engineering Conference*, vol. 1, pp. 582-586, 6-8 September 2004.

Levi, E. (1994), “Iron Core Loss Effects in Indirect Flux Rotor Flux Oriented Induction Machines”, *Proceedings of the 7th Mediterranean Electrotechnical Conference*, vol. 2, pp. 766-769, 12-14 April 1994.

Levi, E., Lamine, A., Cavagino, A. (2005), “Detuned Operation of Vector Controlled Induction Machines due to Stray Load Losses”,*Industry Applications Society Conference*, vol. 1, pp. 500-507, 2-6 October 2005.

Levi, E., Lamine, A., Cavagino, A. (2006), “Impact of Stray Load Losses on Vector Control Accuracy in Current-Fed Induction Motor Drives”, *IEEE Transactions on Energy Conversion*, vol. 21, no. 2, pp. 442-450.

Levi. E., Boglietti A., Lazzari, M. (1995), “Comparative Study of Detuning Effects in Indirect Rotor Flux Oriented Induction Machines Due to Iron Core Losses”, *Proceedings of the International Conference on Power Electronics and Drive Systems*, vol. 2, pp. 639-644, 21-24 February 1995.

Loddick, S.J. (1996), “Modelling Frequency Dependency of Induction Machine Equivalent Circuit Parameters”, *IEE Conference on Power Electronics and Variable Speed Drives*, no. 429, 23-25 September 1996.

Manyage, M.J., Mthombeni, T.L., Pillay, P. & Boglietti, A. (2007), "Improved Prediction of Core Losses in Induction Motors", *IEEE International Electric Machines & Drives Conference*, vol.1, no., pp. 531-536, 3-5 May 2007.

McPherson, G. & Laramore, R.D. (1990), “An Introduction to Electrical Machines and Transformers”, 2nd Edition, Toronto, ON: John Wiley & Sons, Inc., ISBN 0-471-51734-8.

Moon, S.I. & Keyhani, A.(1993), “Estimation of Induction Machine Parameters from Standstill Time Domain Data”, *IEEE IAS Annual Meeting*, vol.1, pp. 336-342, 2-8 Oct. 1993.

Morgan, T.H., Brown, T.E. & Schumer, A.T. (1939), “Reverse-Rotation Test for the Determination of Stray-Load Loss in Induction Machines”, *Transactions of the AIEE*, vol. 58, pp. 319-324.

Mthombeni, T.L. & Pillay, P. (2003), “Core losses in motor laminations exposed to high freqneucy of non-sinusoidal excitation”, IEEE 38th IAS Annual Meeting, vol. 2, pp. 1090-1097, 12-16 Oct 2003.

Nakamura, N. (2006), "A practical method to transform frequency dependent impedance to time domain", *Earthquake Engineering and Structural Dynamics*, vol. 35, pp. 217-231.

Odok, A. (1958), "Stray-load Losses and Stray Torques in Induction Machines", *Transactions of the AIEE*, vol. 77 pt. II, p. 43-53.

Olin, E.M. (1912), "Determination of Power Efficiency of Rotating Electrical Machines. Summation of Losses Versus Input-Output Method", *Transactions of the AIEE*, vol. XXXI part II, pp. 1695-1719.

Repo, A.K. & Arkkio A. (2006), "Parameter Estimation of Induction Machines Using the Numerical Impulse Method", *Proceedings of the International Symposium on Power Electronics, Electrical Drives, Automation and Motion (SPEEDAM)*, pp. 943-948, 23-26 May 2006.

Repo, A.K. (2008), "Numerical Impulse Response Tests to Identify Dynamic Induction-Machine Models", Doctoral Dissertation, Helsinki University of Technology, Department of Electrical Engineering, TKK-DISS-2447, ISBN 978-951-22-9275-2, [Available Online: http://lib.tkk.fi/Diss/2008/isbn9789512292752].

Schwarz, K.K (1964), "Survey of basic stray losses in squirrel-cage induction motors", *Proceedings of the IEE*, vol. 111, no. 9, pp. 1565-1574.

Sellschopp, F.S. & Arjona, M.A. (2007), "Semi-analytical method for determining d-axis synchronous generator parameters using the DC step voltage test", IET Electric Power Applications, vol. 1, no. 3, pp. 348-354, May 2007.

Sousa, G.C.D., Bose, B.K., Cleland, J., Speigel, R.J. & Campbell, P.J. (1992), "Loss Modeling of converter Induction Machine System for Variable Speed Drive", *Proceedings of the International Conference on Industrial Electronics, Control, Instrumentation, and Automation*, vol. 1, pp. 114-120, 9-13 November 1992.

Spooner, E. (1982), "Stray loss in solid-rotor induction machines", *Proceedings of the IEE*, vol. 129, part B, no. 4, pp. 181-189.

Stanley, H.C. (1938), "An analysis of the induction motor", *Transactions of the AIEE*, vol. 57, pp. 751-755.

Steinmetz, C.P. (1892), “On the Law of Hysteresis”, *Transactions of the American Institute of Electrical Engineers*, vol. 9, pp. 3-64.

Storn, R. & Price, K. (1997), “Differential Evolution - a Simple and Efficient Heuristic for Global Optimization over Continuous Spaces”, *Journal of Global Optimization*, Kluwer Academic Publishers, Vol. 11, pp. 341 - 359.

Storn, R. (2008), “Differential Evolution Homepage”, [Available Online: http://www.icsi.berkeley.edu/~storn/code.html#basi], Accessed October 14, 2008.

Yamamoto, S., Gotou, T. & Ara, T. (2004), “Prediction of the Operational Impedance of Rotating Machines by Various DC Testing Methods”, Electrical Engineering in Japan, vol. 147, no. 4, pp. 51-59.

Appendix A

Core Losses in 37kW Caged Induction Motor

FE models, which included hysteretic materials, were used to determine core losses for the 37kW caged induction machine operating at various voltage and frequency points. Note that the flux for the machine was given an upper limit based on rated conditions.

Table A1: Core Losses Obtained using Hysteretic Materials from FEA

Voltage (V)	Frequency (Hz)	Core Losses (W)	Current (A)
50	25	1.53E+01	5.67E+00
100	25	4.87E+01	1.13E+01
100	50	3.79E+01	5.67E+00
150	25	9.70E+01	1.72E+01
200	100	1.04E+02	5.67E+00
200	25	1.54E+02	2.81E+01
200	50	1.25E+02	1.13E+01
225	25	1.82E+02	4.30E+01
300	50	2.54E+02	1.72E+01
400	100	3.55E+02	1.13E+01
400	200	3.12E+02	5.67E+00
400	50	4.18E+02	2.81E+01
450	100	4.39E+02	1.28E+01
450	200	3.89E+02	6.38E+00
450	300	3.59E+02	4.25E+00
450	400	3.39E+02	3.19E+00
450	500	3.25E+02	2.55E+00
450	50	5.04E+02	4.30E+01

Appendix B

Parameters for Finite Element Analysis

MESH is the FE mesh generator for radial flux electrical machines. Its parameters are given in the following table.

Table B1: MESH parameters

Basic mesh of stator and rotor slot pitch	82
Order of elements	2
Number of elements	1516
Number of nodes	3085
Elements in the stator	528
Elements in the rotor	812
Elements in the air gap	176
Nodes in the stator	1185
Nodes in the rotor	1723
Nodes in the air gap	177

CIMAC is a program that conducts FE analysis of time-harmonic AC field and circuit equations of cage induction motors. Non-linear materials are modelled by an effective reluctivity. Input power, air-gap torque, resistive stator and rotor losses are calculated. Its parameters are given in the following table.

Table B2: CIMAC Parameters

Source type	Voltage
End ring impedances included	Y
Rotation angle	0°
Stator connection	Star
Applied Voltage	Various
Slip	0 (no load)
Stator temperature	100°
Rotor temperature	120°

CIMTD is the program that conducts time-stepping finite element analysis for electrical machines. The circuit equations for the stator winding, field winding and damping cage are solved with the field equations. The core materials can either be modelled using

single-valued or non-single valued (hysteretic) magnetisation curves. The non-linearity of the iron is solved using the fixed-point method. The following parameters are used.

Table B3: CIMTD Parameters

Source type	Voltage
End ring impedances included	Y
Rotation angle	0°
Stator connection	Star
Applied Voltage	Various
Slip	0 (no load)
Stator temperature	100°
Rotor temperature	120°

Appendix C

Construction of 37kW Caged Induction Machine

Table C1: Dimensions and Rating of 37kW Caged Induction Machine

Length of laminated core	249
Outer diameter of the stator core	310
Inner diameter of the stator core	200
Number of stator slots	
Outer diameter of the rotor core	198.4
Inner diameter of the rotor core	70.0
Number of rotor slots	40
Stator slot	
h_s	23.9
h_{s1}	1.0
h_{s2}	17.5
b_{s1}	3.5
b_{s2}	6.5
b_{s3}	8.8
Rotor slot	
h_{r1}	0.7
h_{r2}	16.1
h_{r3}	17.8
b_{r1}	6.0
b_{r2}	2.5
b_{r3}	5.85
Stator winding	
Number of poles	4
Number of phases	3
Number of parallel paths	2
Number of turns per slot	12
Coil pitch in slot pitches	12
Resistance of stator phase at 80 °C (Ω)	0.079
Rated power (kW)	37
Rated voltage (V)	380
Rated current (A)	73
Rated frequency (Hz)	50
Rated slip (%)	0.02

The stator and rotor slot dimensions and their basic mesh models are shown below.

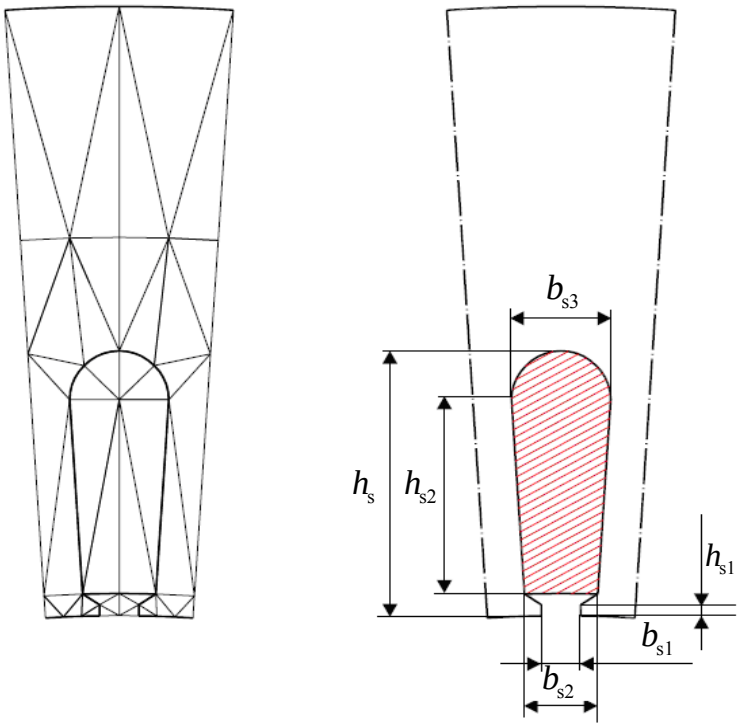

Figure C1: Stator Slot Dimensions

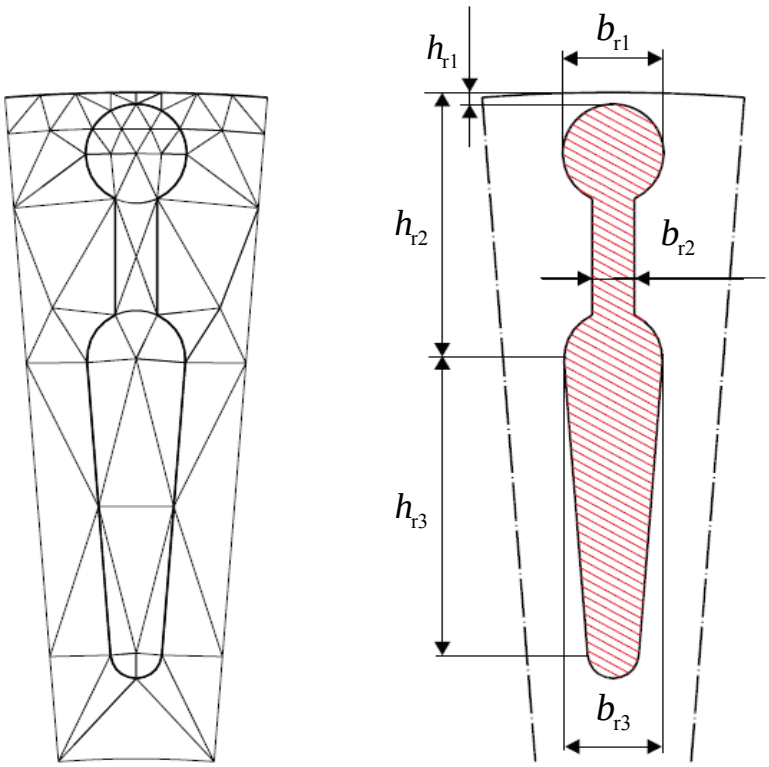

Figure C2: Rotor Slot Dimensions